Supporting Information for

Boosting the Catalytic Performance of Metalloporphyrin-Based Covalent Organic Frameworks via Coordination Engineering for CO_2 and O_2 Reduction

*Zhixin Ren, Ke Gong, Bo Zhao, Shi-Lu Chen, Jing Xie**

Key Laboratory of Cluster Science of Ministry of Education, Beijing Key Laboratory of Photoelectronic / Electrophotonic Conversion Materials, School of Chemistry and Chemical Engineering, Beijing Institute of Technology, Beijing, 100081, China.

E-mail: jingxie@bit.edu.cn

Contents

Supplementary Note 1. Additional details for Machine Learning

We tested the predictive ability of the trained ML models for Por-COFs with other central metals, Cu for CO_2RR and Pt for ORR.[1-4] For each metal, the values of U_L^{CO2RR} and η^{ORR} were predicted for six types of coordination environment, i.e. N_4, N_3O, N_3S, N_2O_2, N_2S_2, N_2OS (Table S15). Among them, Cu-N_3S-Por-COF exhibits the optimal CO_2RR activity (U_L^{CO2RR} = −0.81 V); and the Pt-N_2S_2-Por-COF exhibits the optimal ORR activity (η^{ORR} = 0.64 V). It turns out these two ML-predicted values differ with the DFT calculated values by −0.67 and 0.97 V (Figure S21). We further used the trained GBR-ML model to predict the U_L^{CO2RR} value of Co-N_3C_1 and Co-N_2C_2-Por-COF system.[5] Note that the coordinated carbon-atom was not in the training set. Inspiringly, it correctly predicted the catalytic order of Co-N_2C_2 > Co-N_3C_1, albeit the match between ML-predicted and DFT calculated U_L^{CO2RR} value is mediocre (error is 0.38 V). Above tests suggest that the trained model is immature to predict properties of systems that are out of the training set, which is usually the case. A direction to improve the accuracy of the model is to increase the sample size and type.

Supplementary Figures

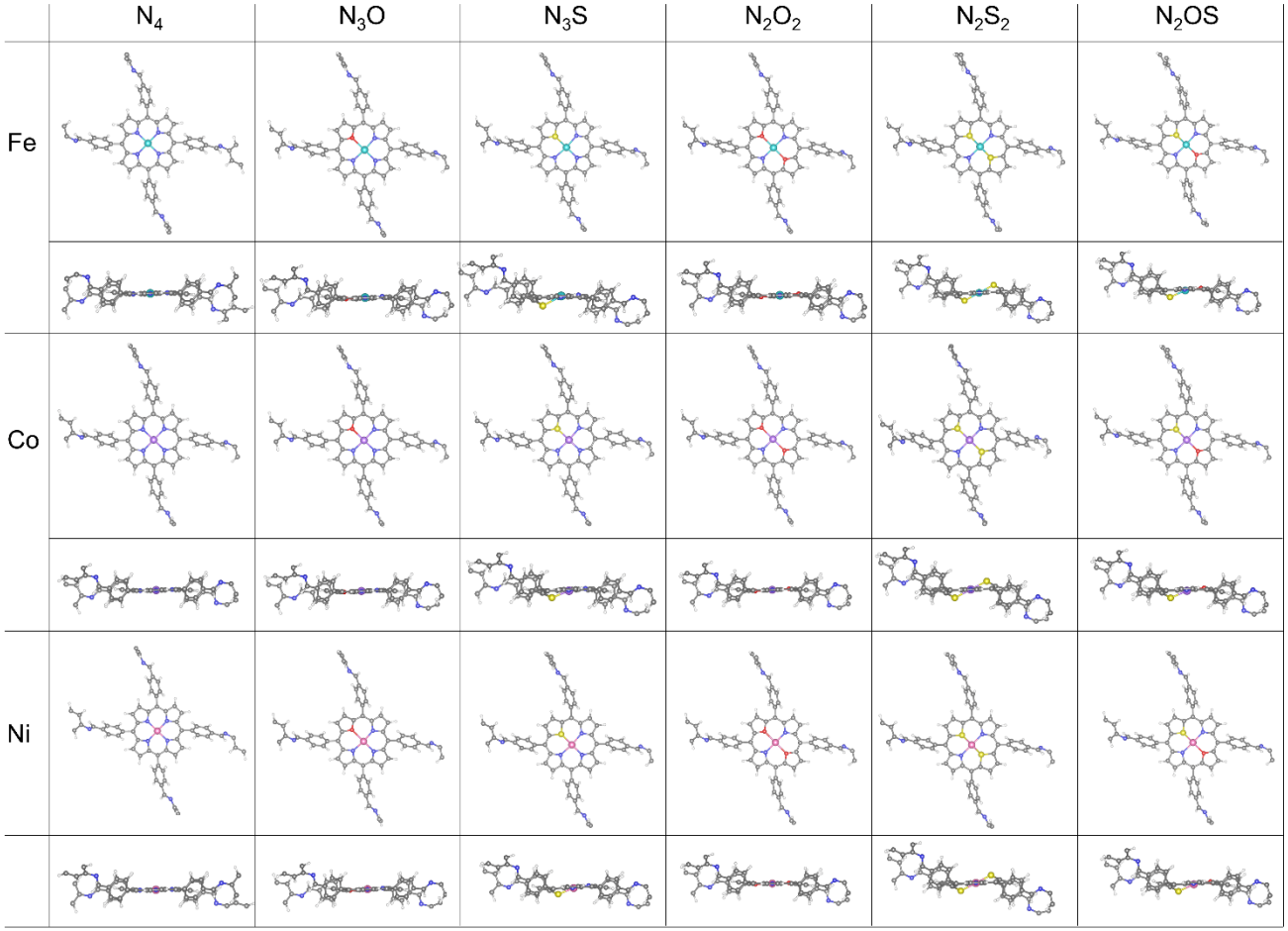

Figure S1. Optimized structures of Fe/Co/Ni-N_xO_y-Por-COFs. Color code: C, grey; N, blue; O, red; S, yellow; H, white; Fe, cyan; Co, purple; Ni, pink.

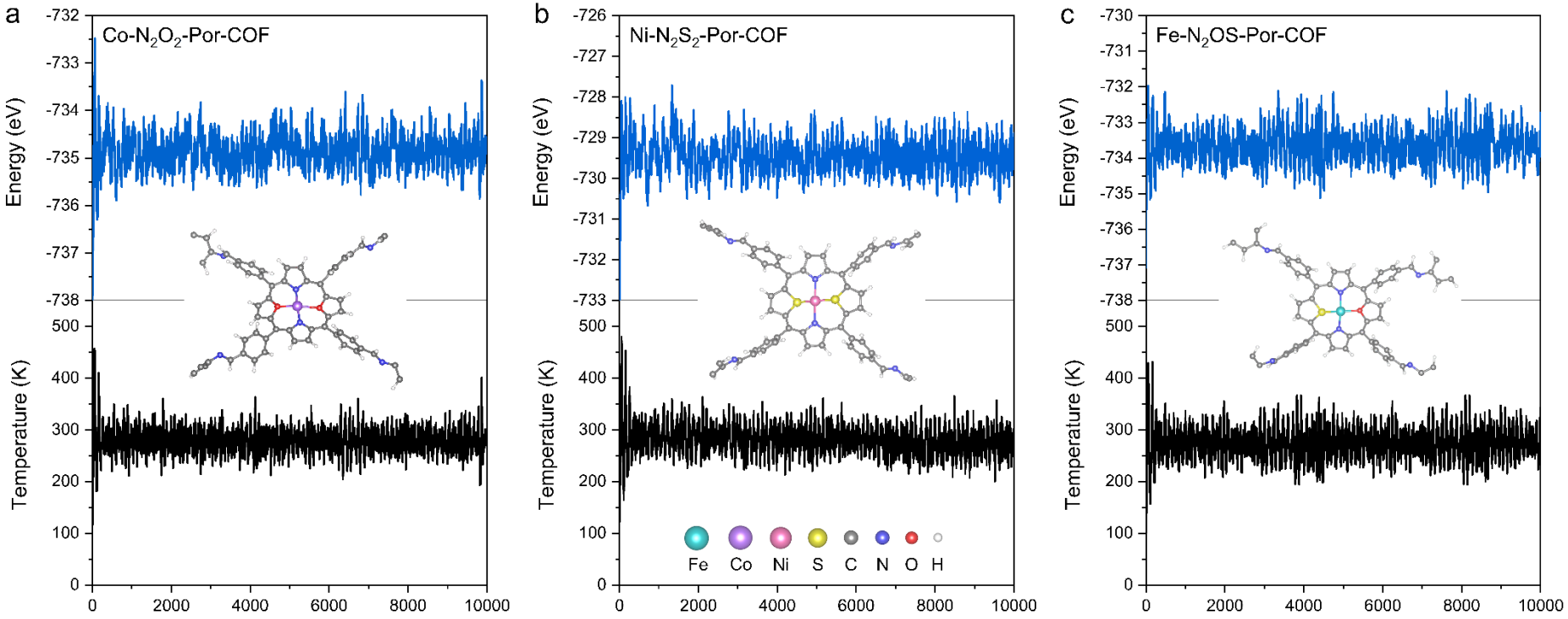

Figure S2. Total energy and temperature evolutions versus the time of AIMD simulation for a) Co-N_2O_2-, b) Ni-N_2S_2- and c) Fe-N_2OS-Por-COFs. Snapshots of the equilibrium structures are inserted.

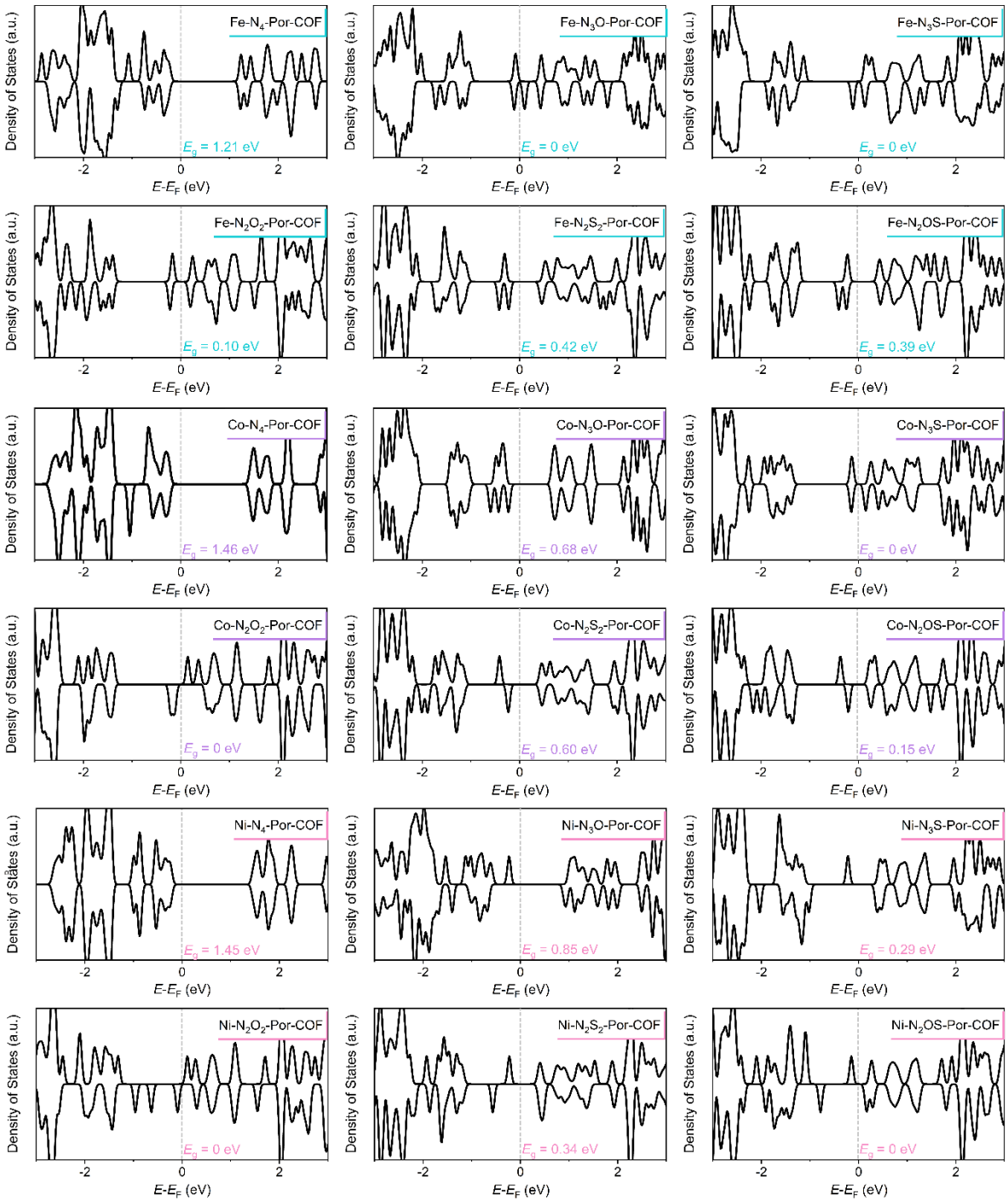

Figure S3. Density of states of the Fe/Co/Ni-$N_xO_yS_z$-Por-COFs. The Fermi energy is referenced at 0 eV.

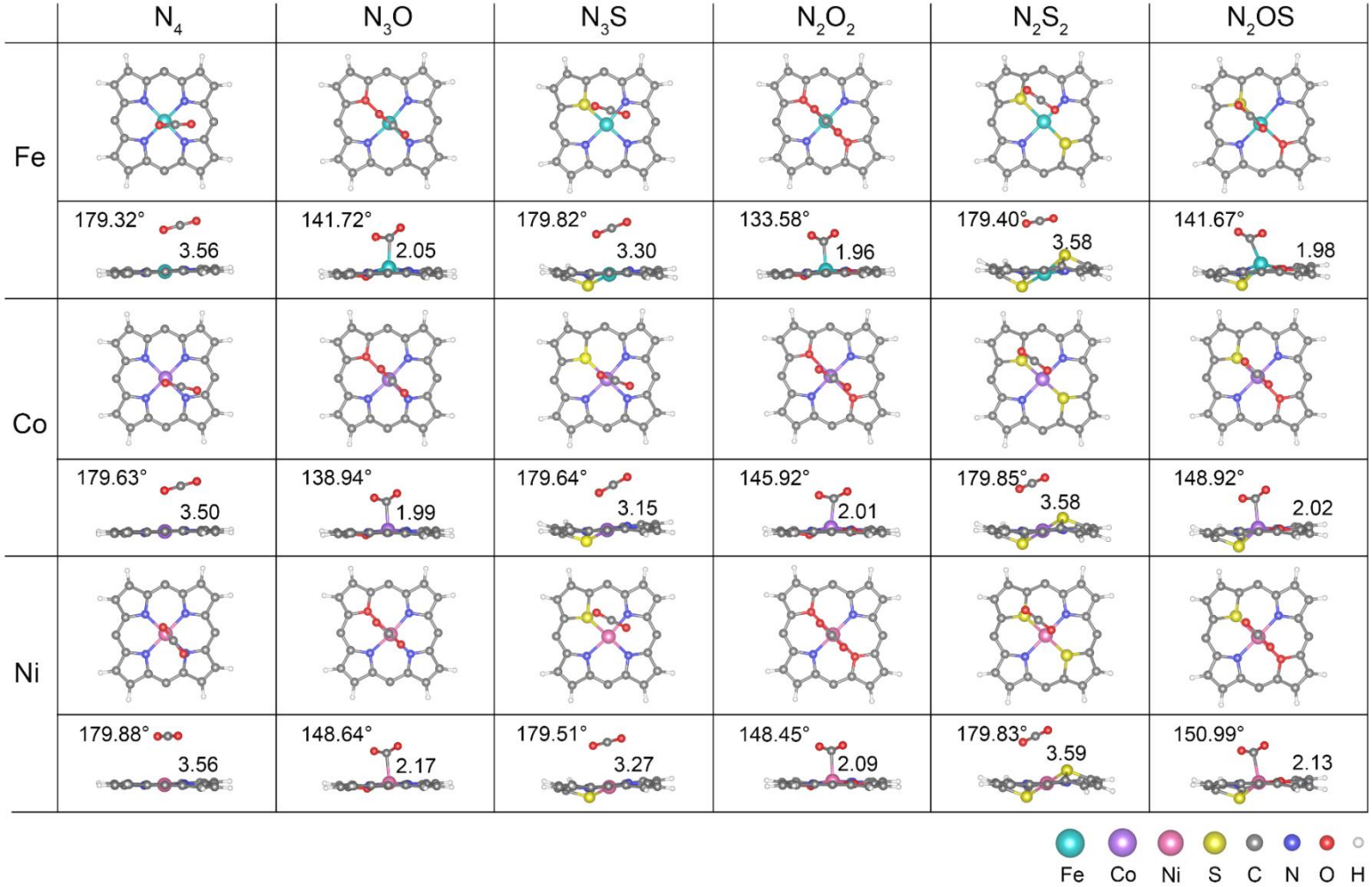

Figure S4. Stable configurations for *CO_2 adsorbed on Fe/Co/Ni-$N_xO_yS_z$-Por-COFs. For clarity, the tetraphenyl and the p-phenylenediamine (PPDA) moieties of M-$N_xO_yS_z$-Por-COFs are not shown.

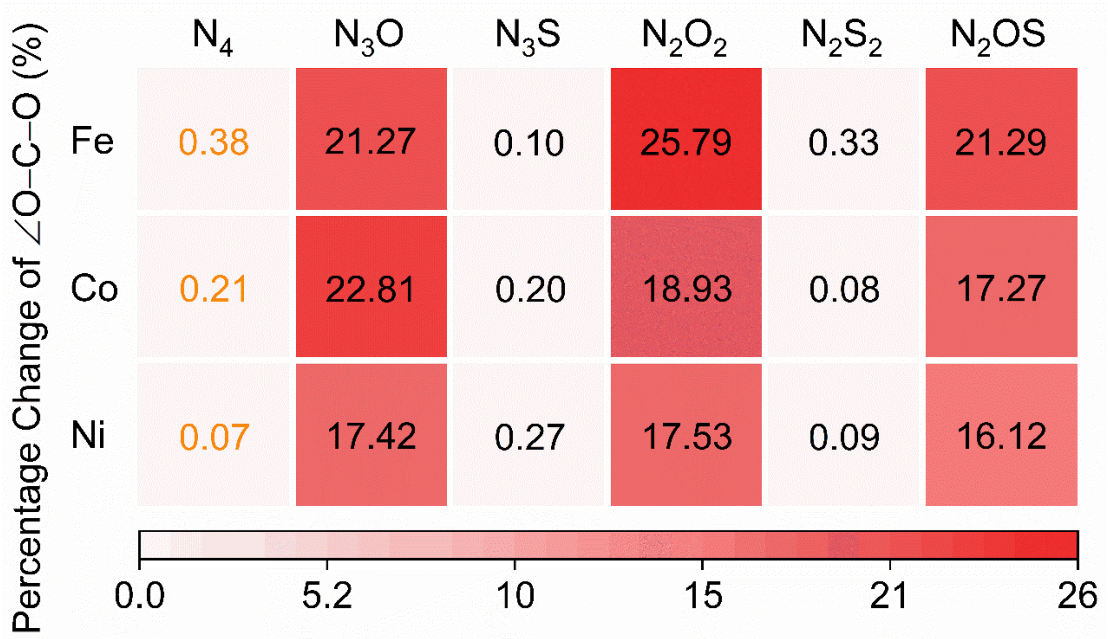

Figure S5. Percentage change in the angle (∠OCO) of absorbed *CO_2 compared to linear CO_2 molecule in the gas phase. Refer to Table S8 for the values of the angle.

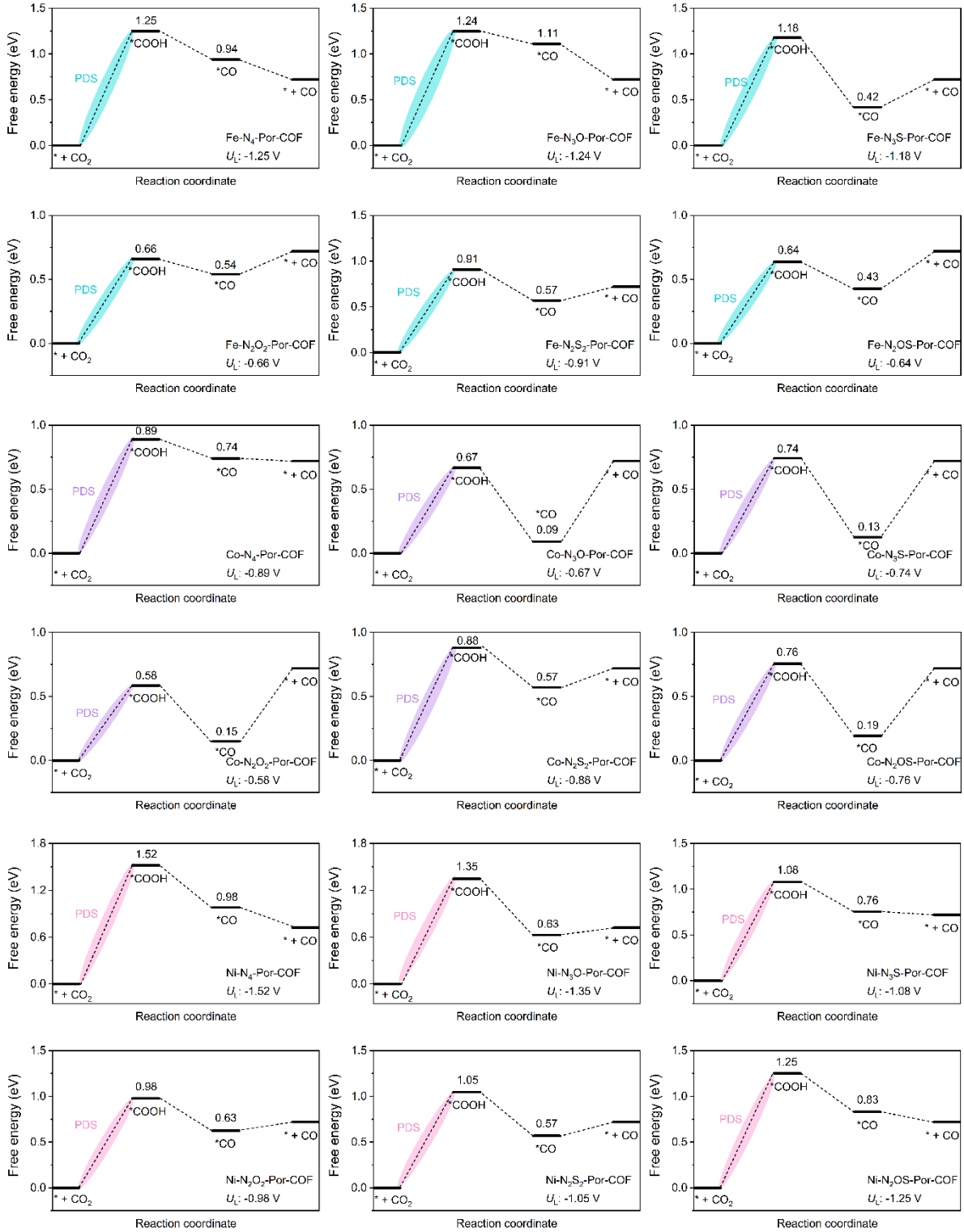

Figure S6. Free-energy diagram for CO_2RR-to-CO on Fe/Co/Ni-$N_xO_yS_z$-Por-COFs.

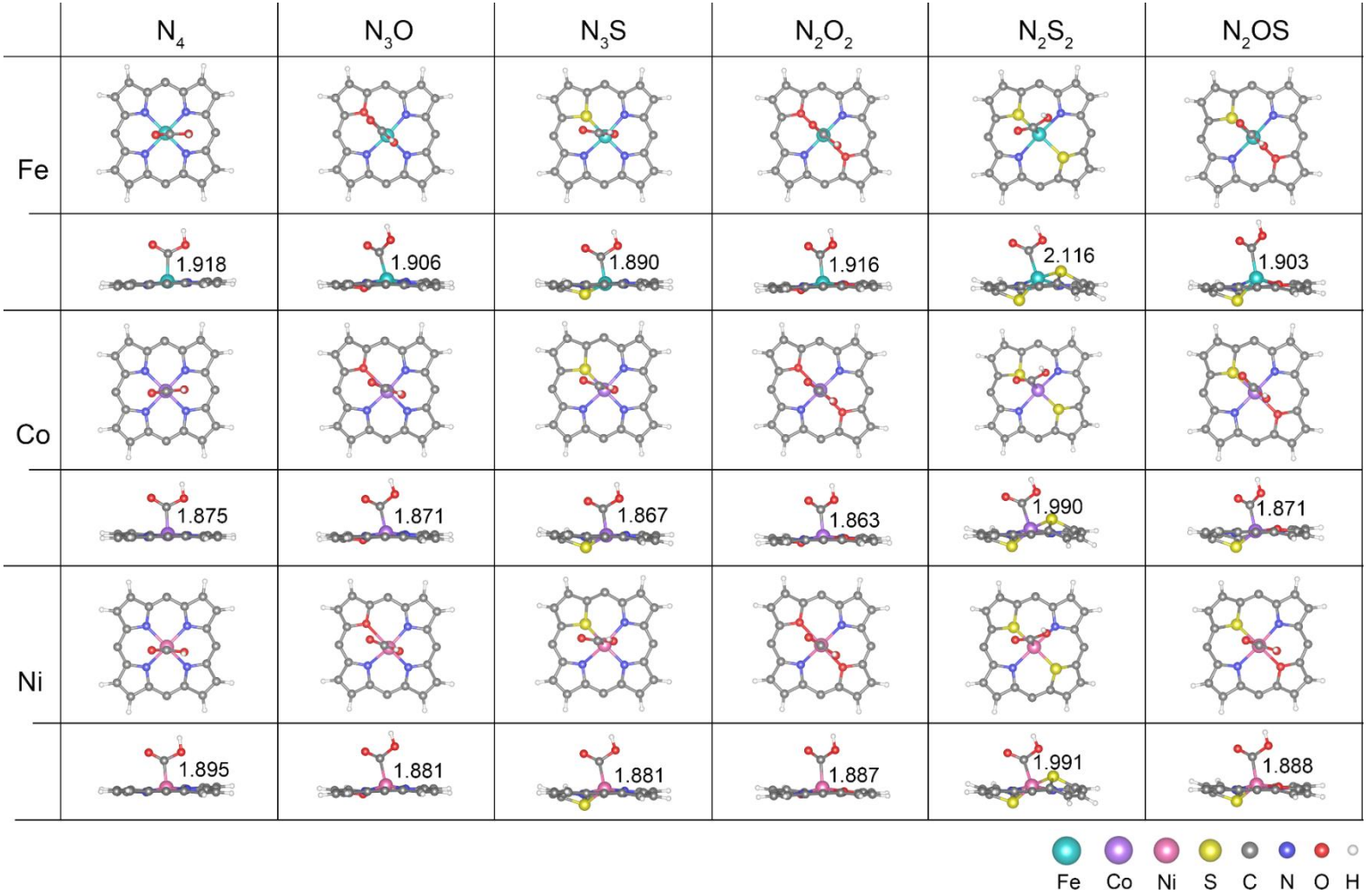

Figure S7. Optimized configurations of the *COOH intermediate on Fe/Co/Ni-$N_xO_yS_z$-Por-COFs. The M−C bond lengths (in Å) are present. For clarity, the tetraphenyl and the p-phenylenediamine (PPDA) moieties of M-$N_xO_yS_z$-Por-COFs are not shown.

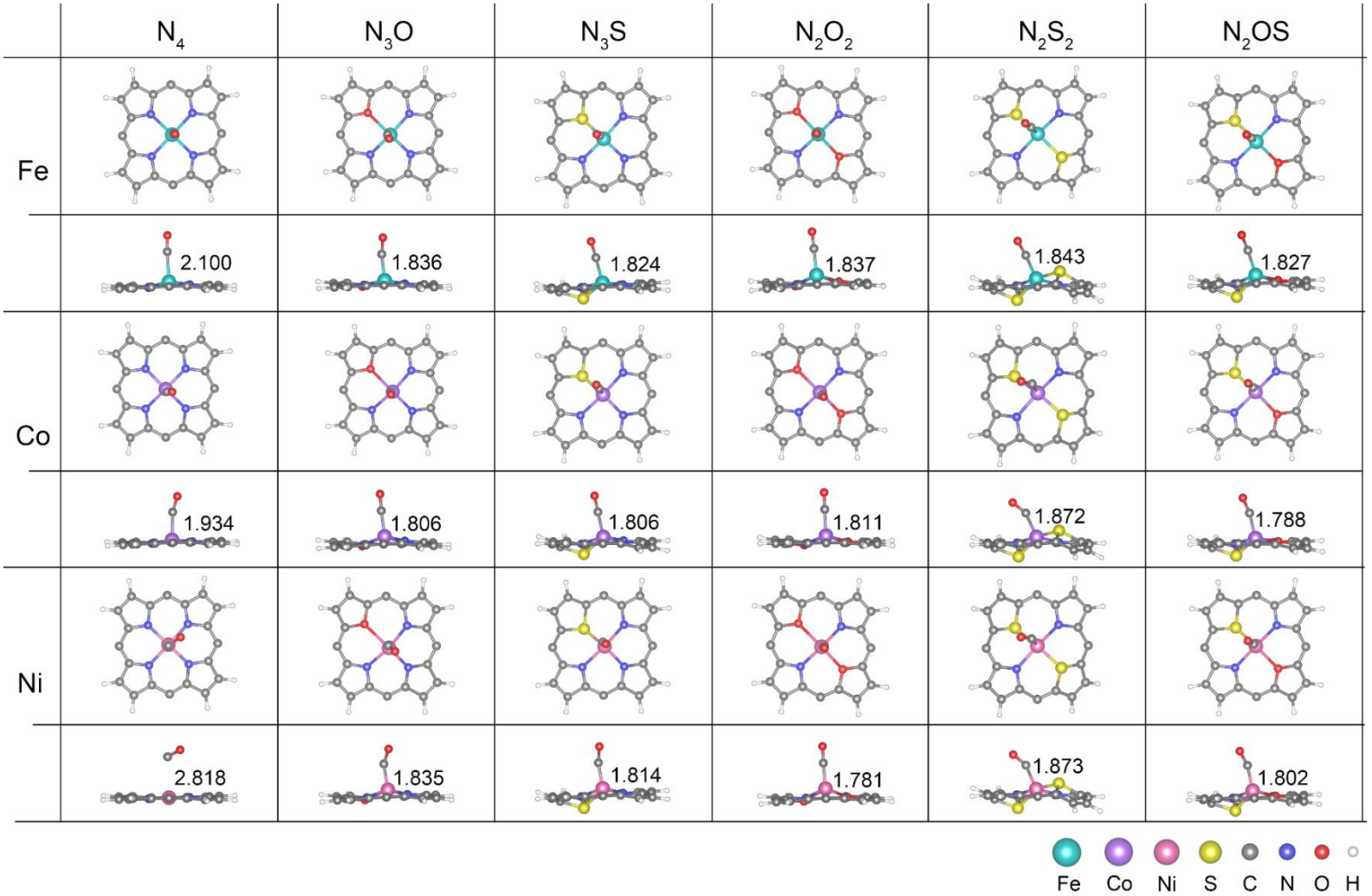

Figure S8. Optimized configurations of the *CO intermediate on Fe/Co/Ni-$N_xO_yS_z$-Por-COFs. The M−C bond lengths (in Å) are present. For clarity, the tetraphenyl and the p-phenylenediamine (PPDA) moieties of M-$N_xO_yS_z$-Por-COFs are not shown.

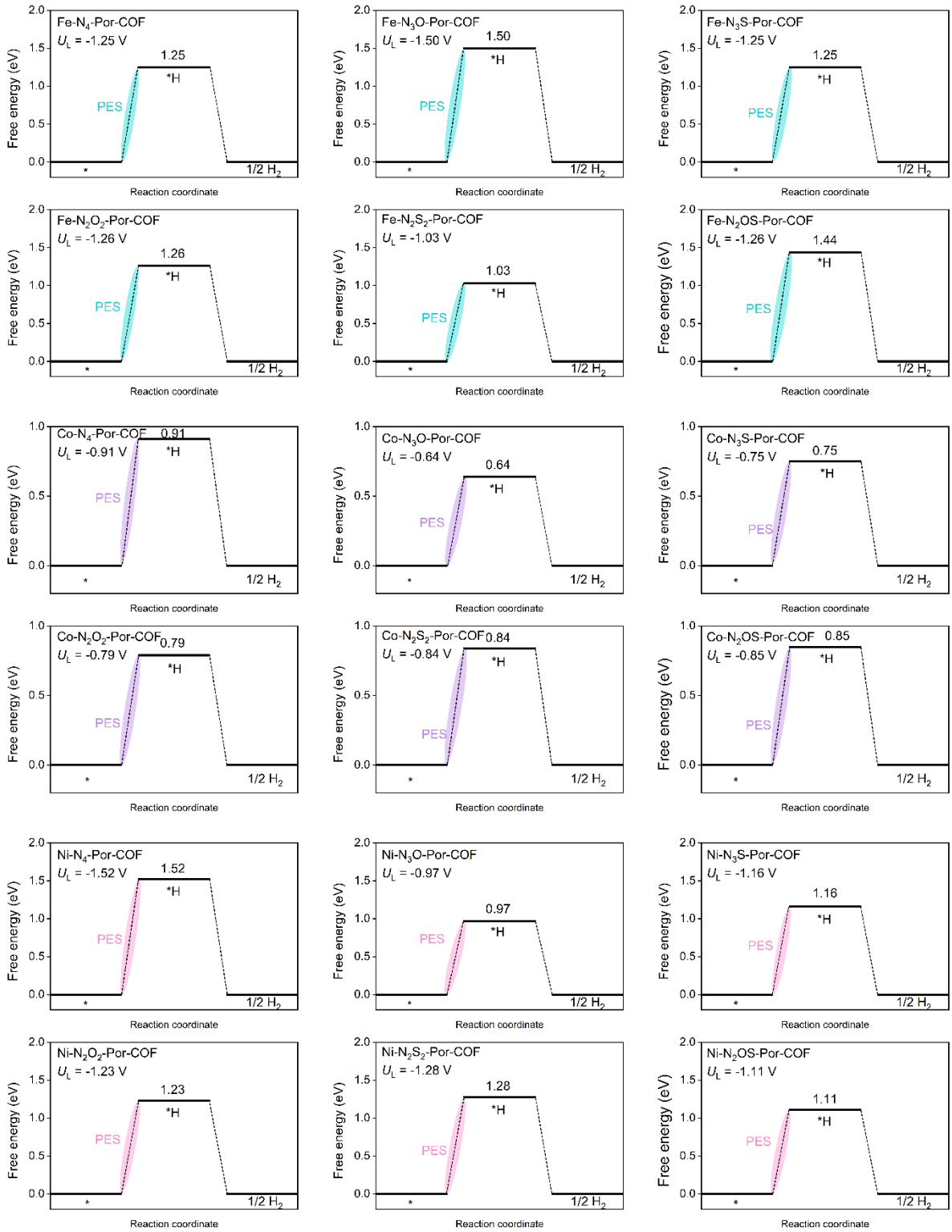

Figure S9. Free-energy diagram for HER on Fe/Co/Ni-$N_xO_yS_z$-Por-COFs.

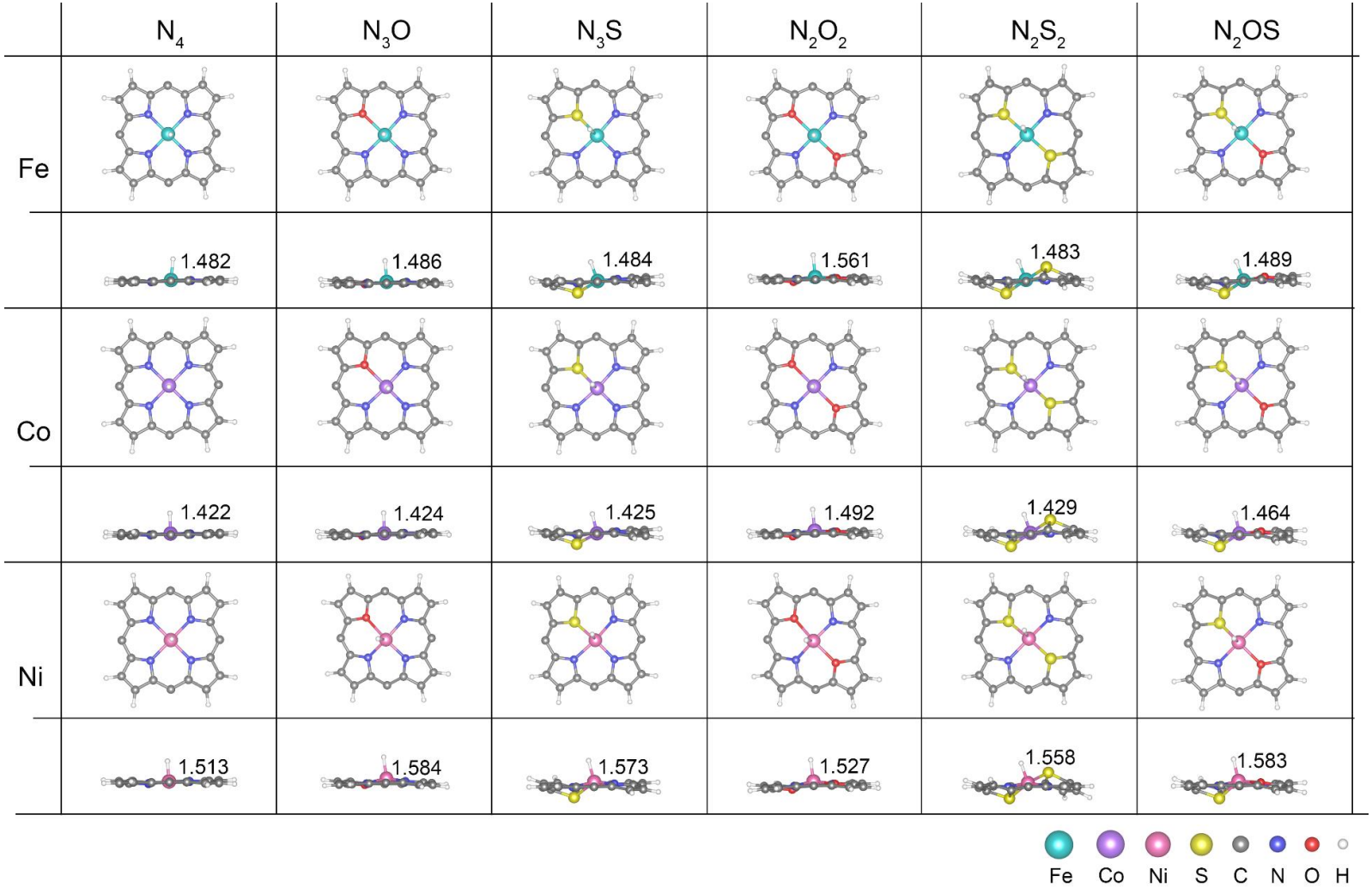

Figure S10. Optimized configurations of the *H intermediate on Fe/Co/Ni-$N_xO_yS_z$-Por-COFs. The M−H bond lengths (in Å) are present. For clarity, the tetraphenyl and the p-phenylenediamine (PPDA) moieties of M-$N_xO_yS_z$-Por-COFs are not shown.

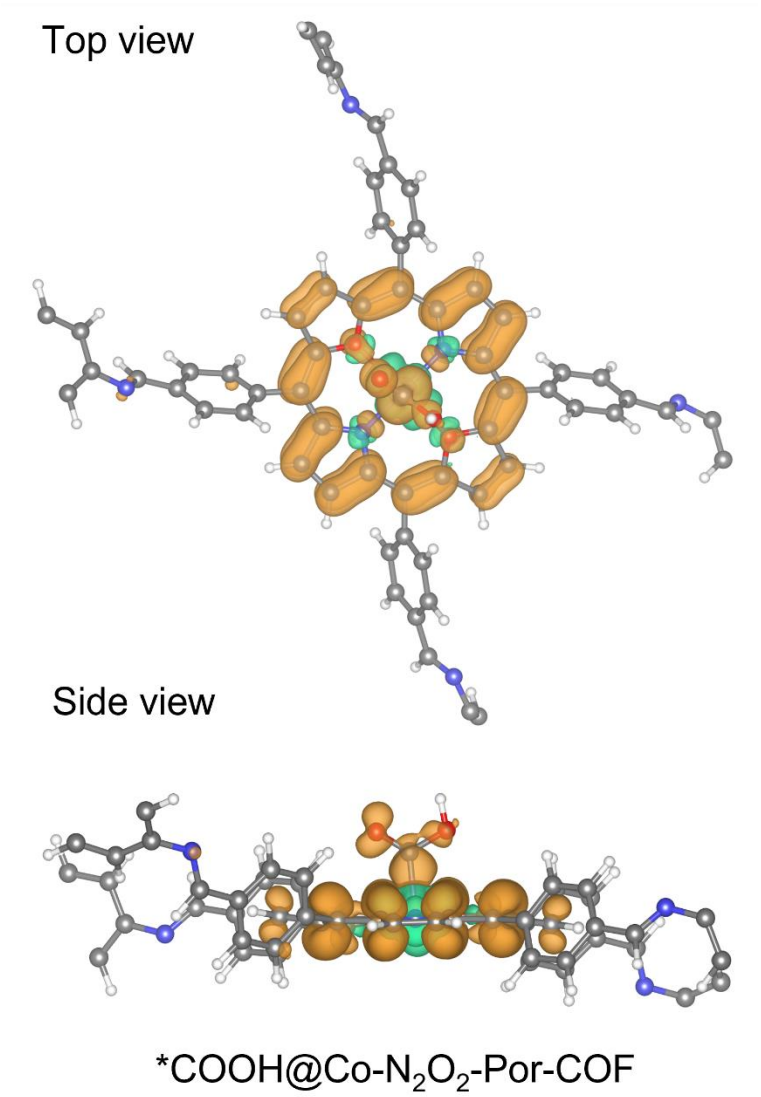

Figure S11. Spin population of COOH@Co-N_2O_2-Por-COF intermediate. Orange and green colors indicate α or β spin electron density, respectively. Isosurfaces of charge density are set to 0.001 e Å $^{-3}$. For clarity, the tetraphenyl and the p-phenylenediamine (PPDA) moieties of Co-N_2O_2-Por-COF are not shown.

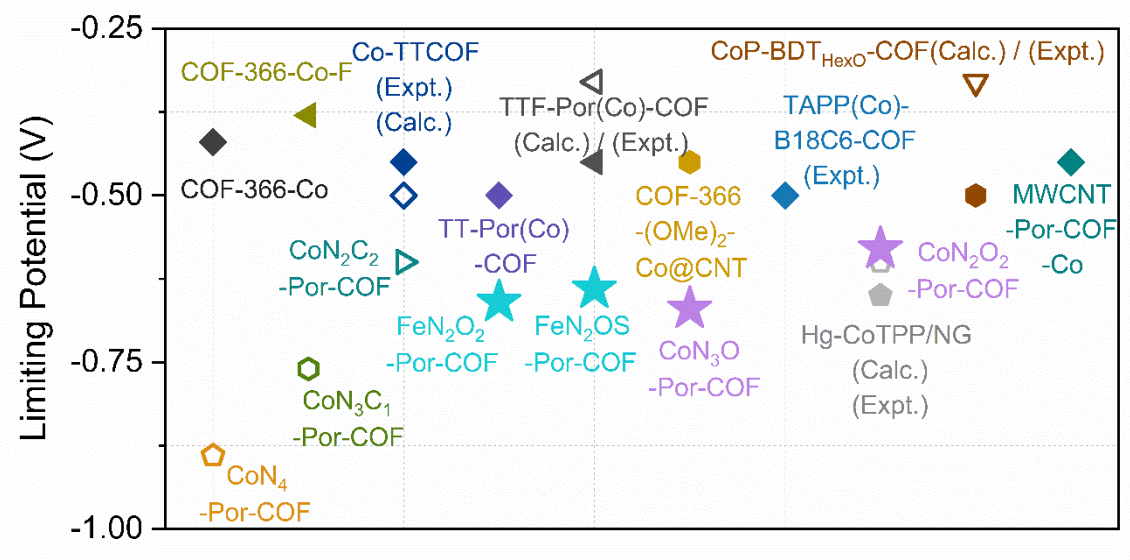

Figure S12. Electrocatalytic CO_2RR performance comparison between the designed Co-N_2O_2-, Fe-N_2OS-, Fe-N_2O_2- and Co-N_3O-Por-COFs (this work) and experimentally synthesized Co-Por-COFs for CO_2-to-CO reduction. The calculated limiting potentials U_L in this work (stars) are compared with experimental onset potentials U^{onset} (solid points) and/or calculated U_L (hollow points) in literatures. [6-15]

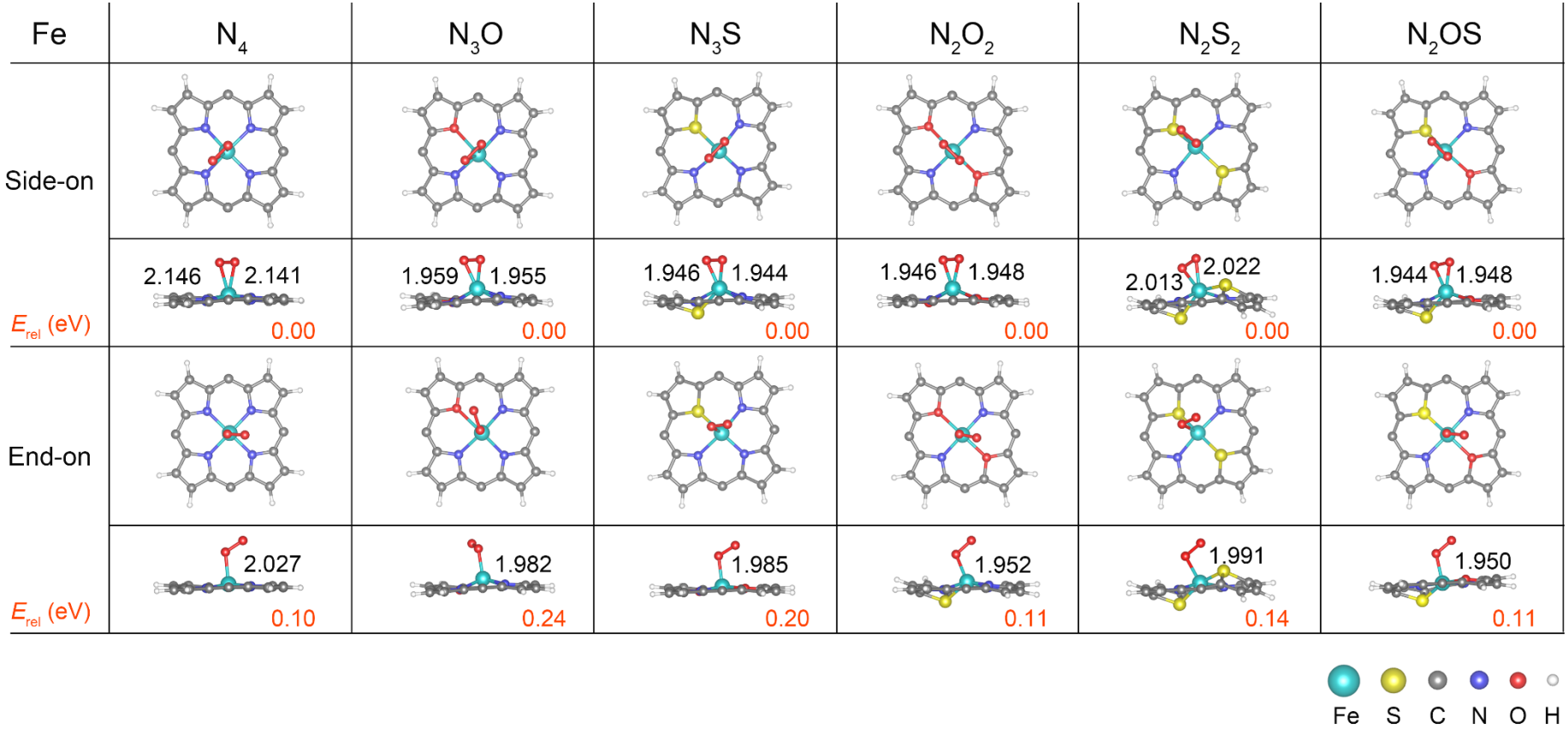

Figure S13. Side-on and end-on type adsorption configurations of $*O_2$ on Fe-$N_xO_yS_z$-Por-COFs. The Fe–O bond lengths (in Å) and relative energies (E_{rel}, in eV) are present. For clarity, the tetraphenyl and the p-phenylenediamine (PPDA) moieties of Fe-$N_xO_yS_z$-Por-COFs are not shown.

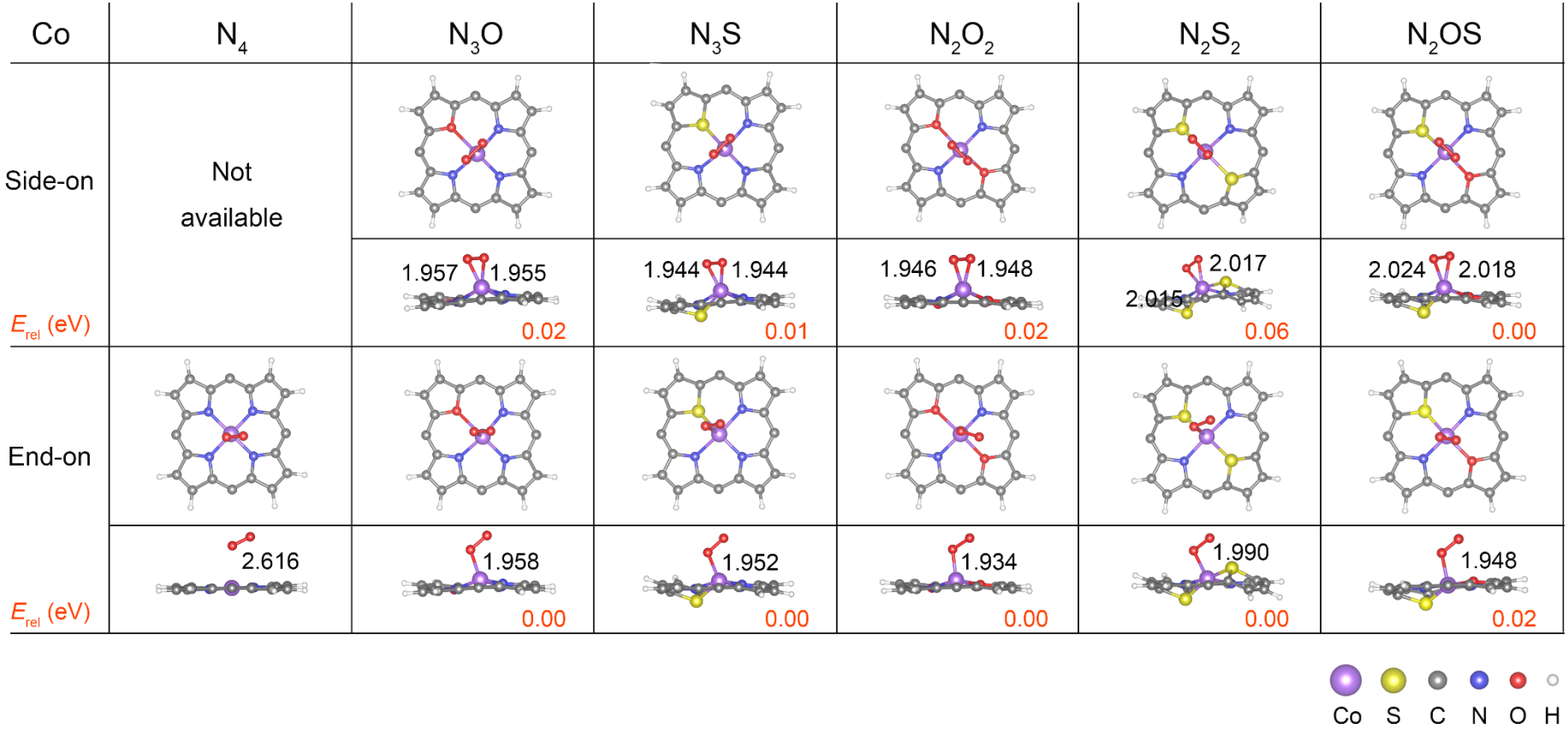

Figure S14. Side-on and end-on type adsorption configurations of $*O_2$ on Co-$N_xO_yS_z$-Por-COFs. The Co–O bond lengths (in Å) and relative energies (E_{rel}, in eV) are present. For clarity, the tetraphenyl and the p-phenylenediamine (PPDA) moieties of Co-$N_xO_yS_z$-Por-COFs are not shown.

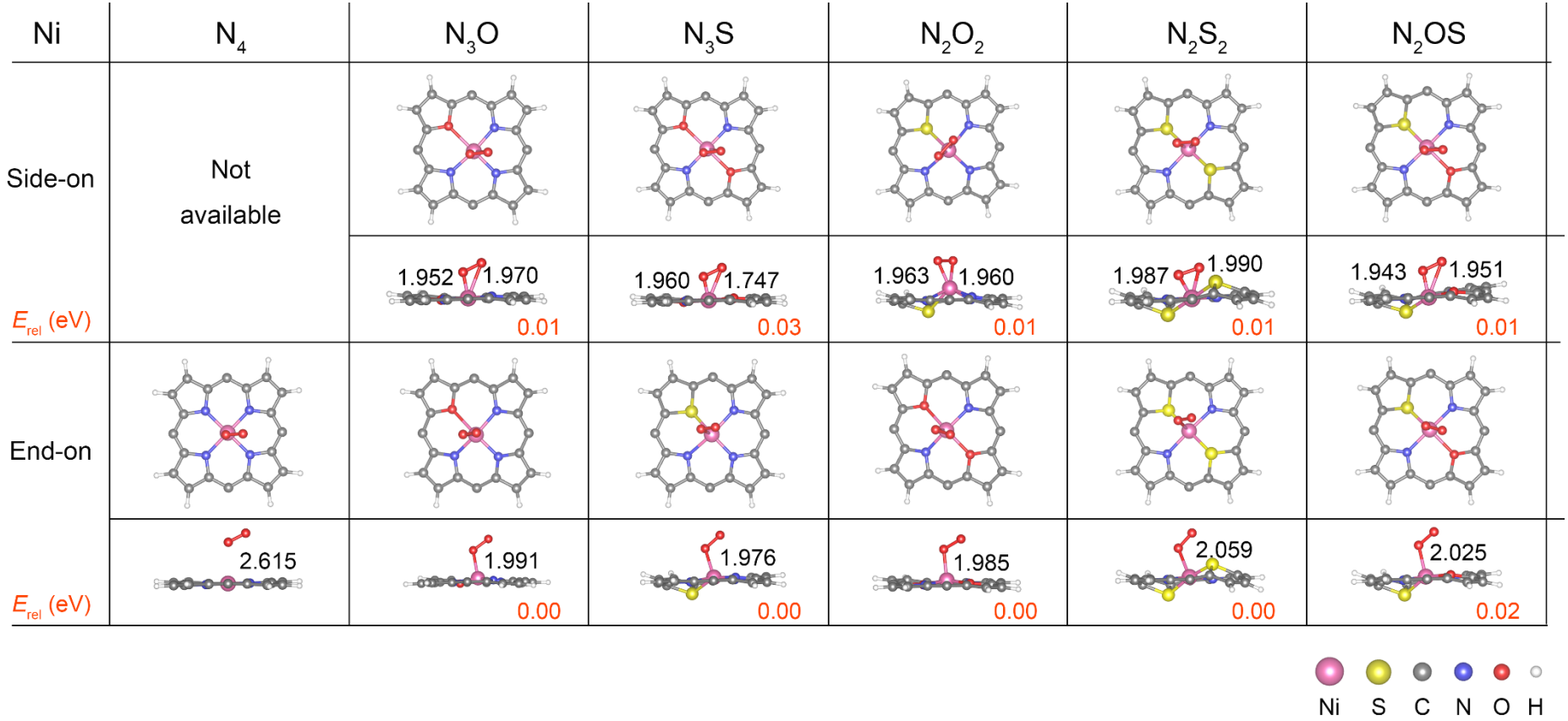

Figure S15. Side-on and end-on type adsorption configurations of $*O_2$ on Ni-$N_xO_yS_z$-Por-COFs. The Co−O bond lengths (in Å) and relative energies (E_{rel}, in eV) are present. For clarity, the tetraphenyl and the p-phenylenediamine (PPDA) moieties of Ni-$N_xO_yS_z$-Por-COFs are not shown.

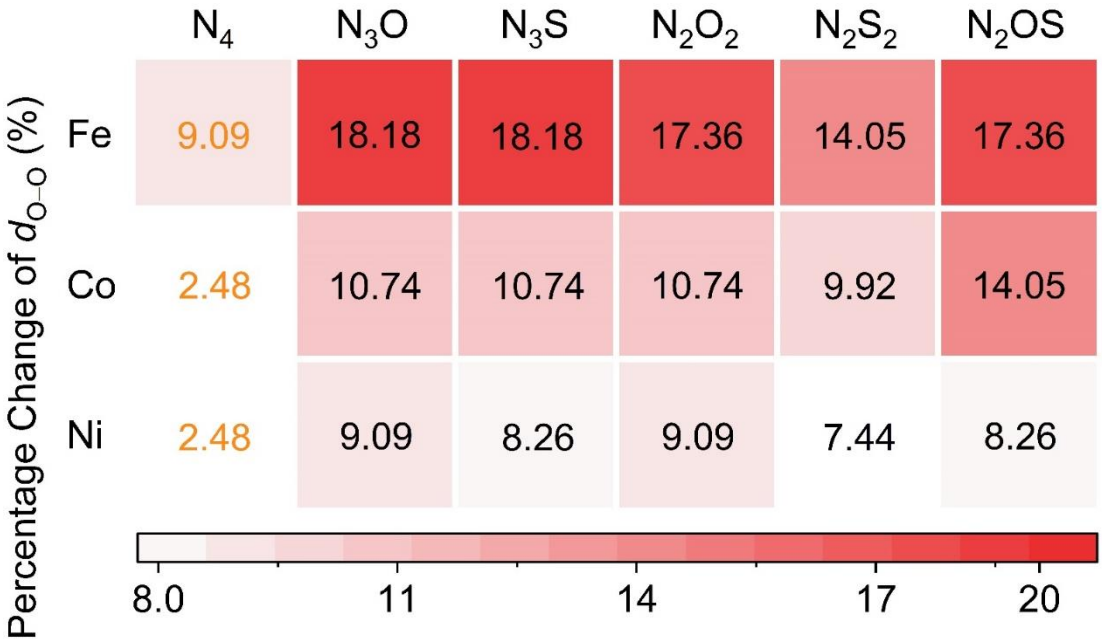

Figure S16. Percentage change in the bond length ($d_{O–O}$) of absorbed *O_2 compared to linear O_2 molecule in the gas phase. Refer to Table S9 for the values of the bond length.

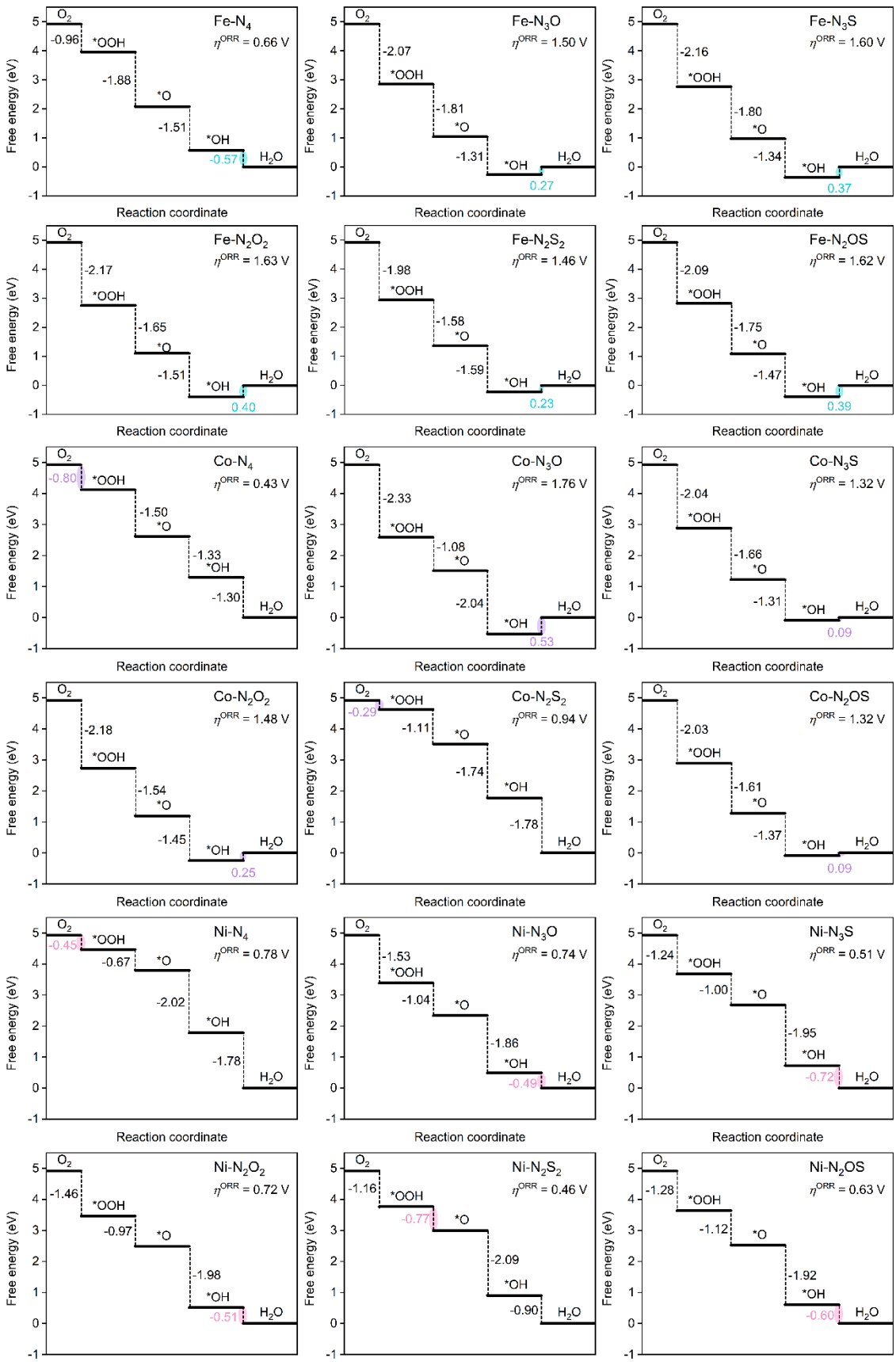

Figure S17. Free energy diagram for 4e$^-$ ORR R on Fe/Co/Ni-$N_xO_yS_z$-Por-COFs (U = 0 V, pH = 0). The colored shadows specify the potential limiting step (PDS).

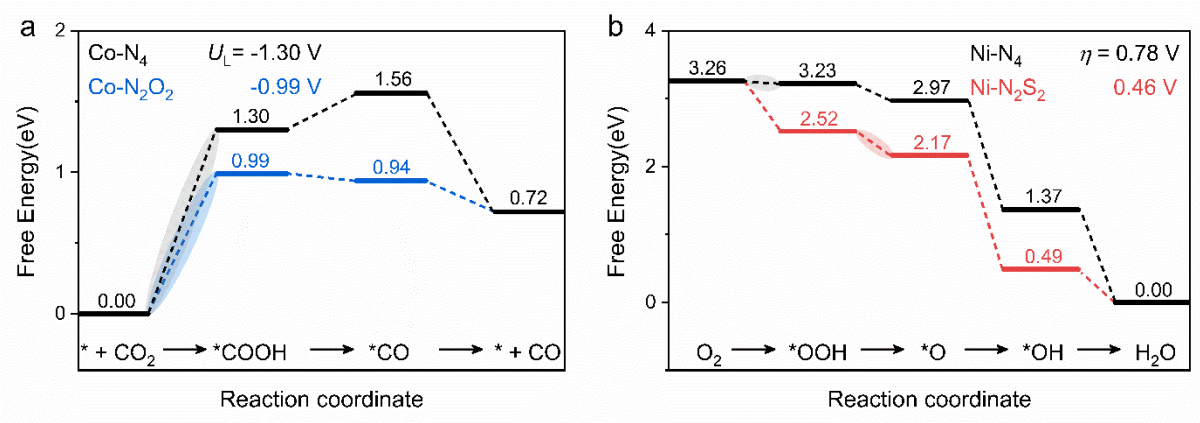

Figure S18. Free energy diagrams that computed at pH = 7 of a) CO_2RR on Co-N_4-and Co-N_2O_2-Por-COFs and b) ORR on Ni-N_4-and Ni-N_2S_2-Por-COFs.

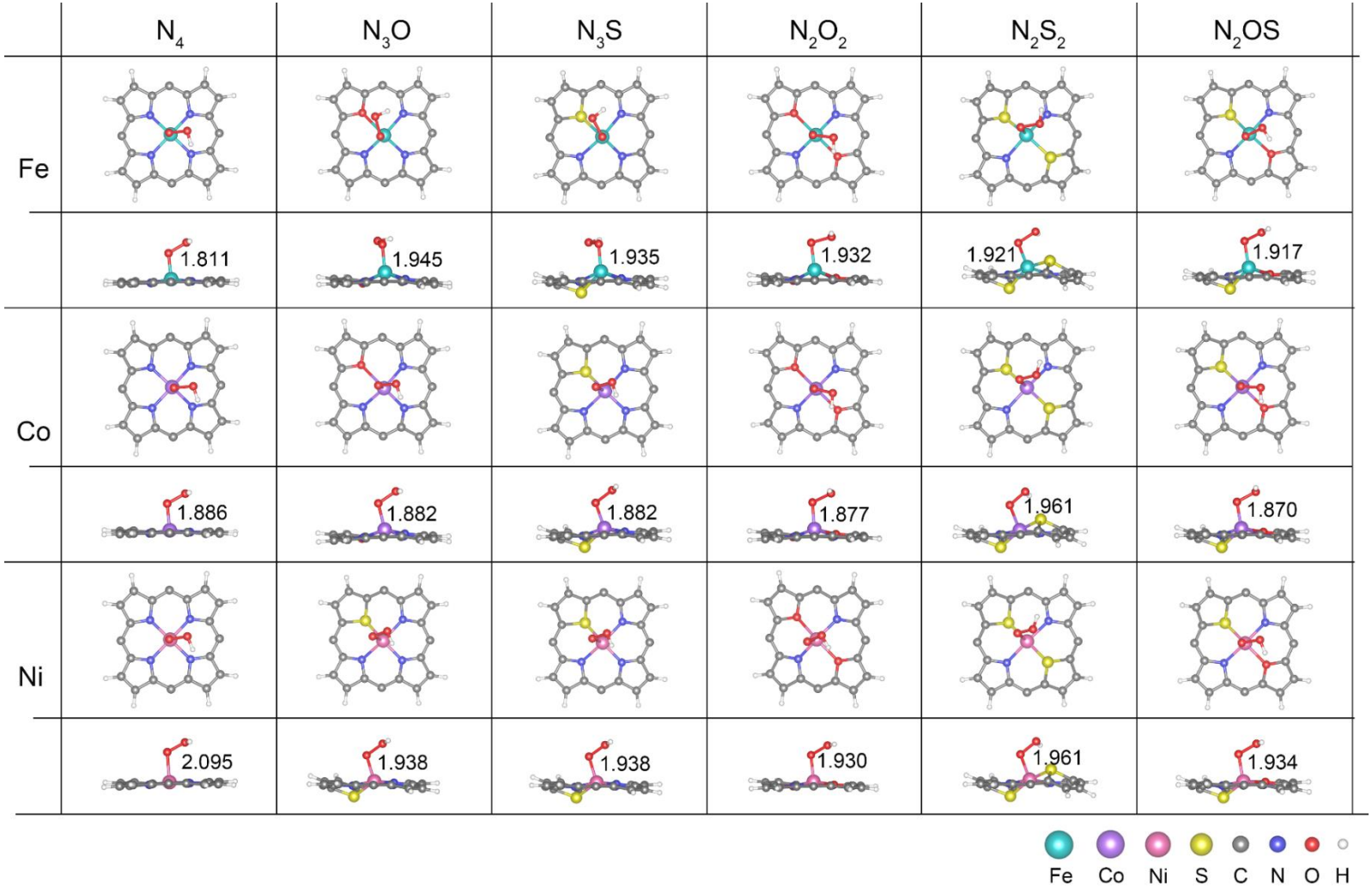

Figure S19. Optimized configurations of the *OOH intermediate on Fe/Co/Ni-$N_xO_yS_z$-Por-COFs. The M−O bond lengths (in Å) are present. For clarity, the tetraphenyl and the p-phenylenediamine (PPDA) moieties of M-$N_xO_yS_z$-Por-COFs are not shown.

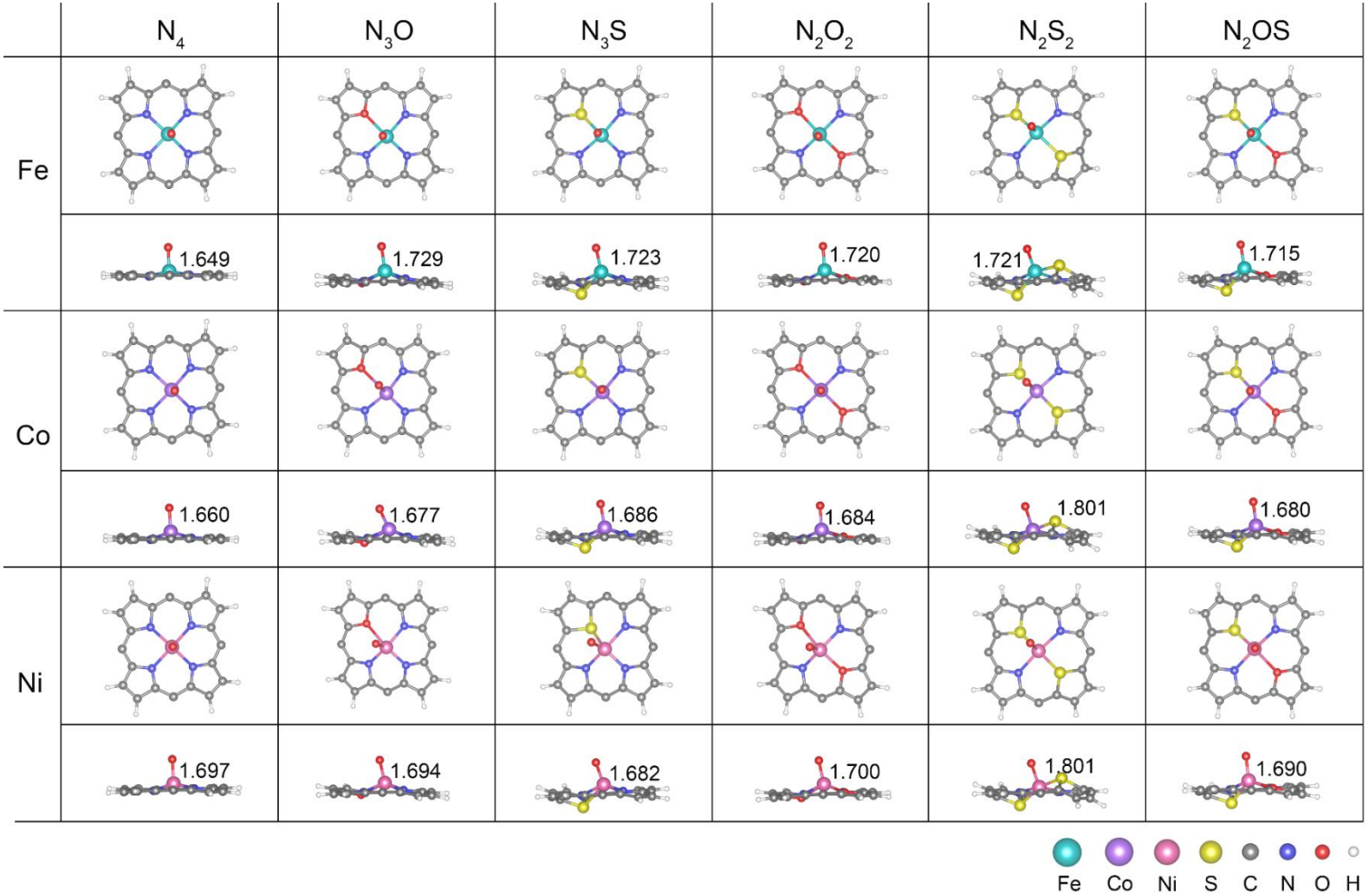

Figure S20. Optimized configurations of the *O intermediate on Fe/Co/Ni-$N_xO_yS_z$-Por-COFs. The M−O bond lengths (in Å) are present. For clarity, the tetraphenyl and the p-phenylenediamine (PPDA) moieties of M-$N_xO_yS_z$-Por-COFs are not shown.

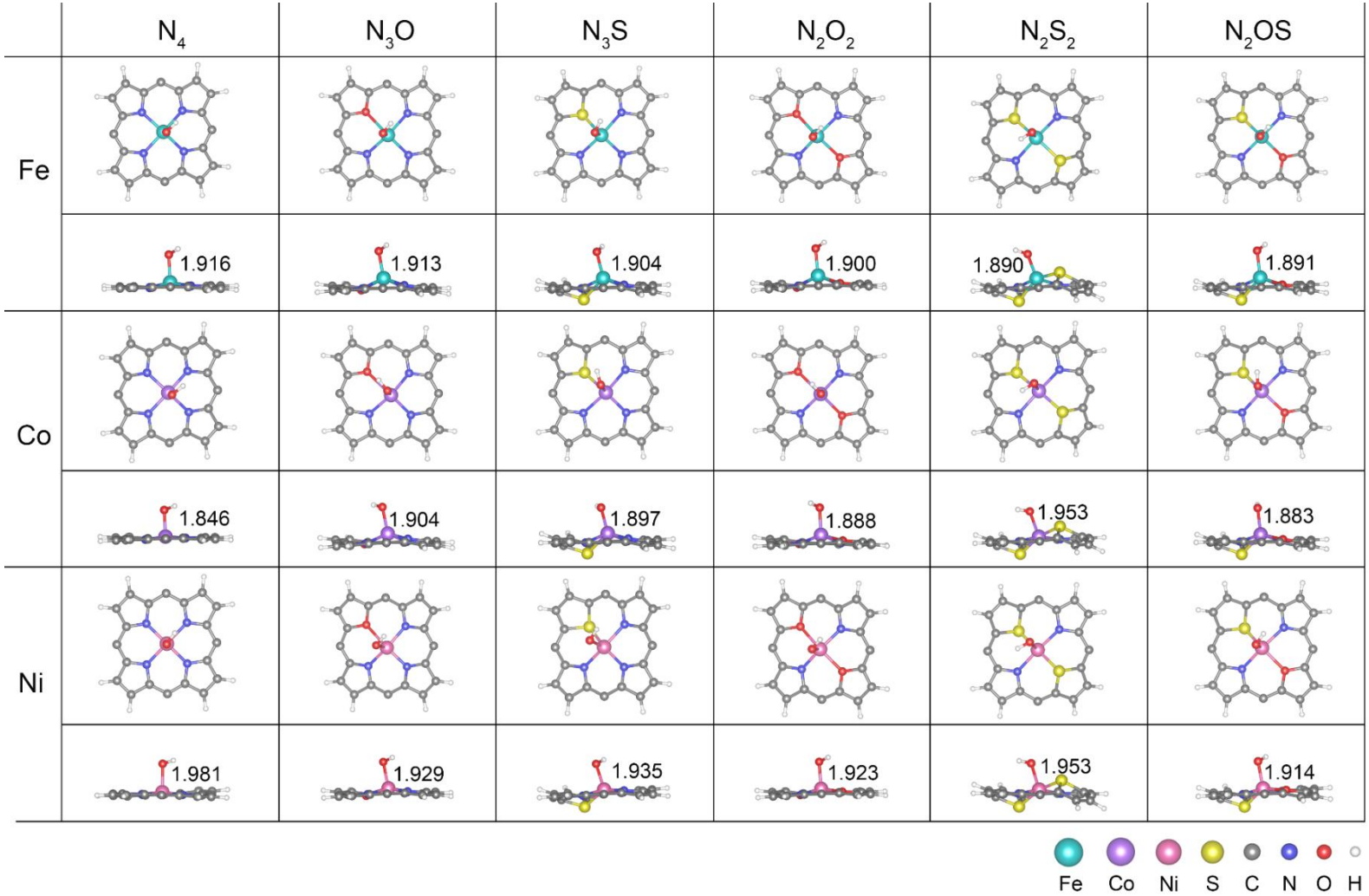

Figure S21. Optimized configurations of the *OH intermediate on Fe/Co/Ni-$N_xO_yS_z$-Por-COFs. The M−O bond lengths (in Å) are present. For clarity, the tetraphenyl and the p-phenylenediamine (PPDA) moieties of M-$N_xO_yS_z$-Por-COFs are not shown.

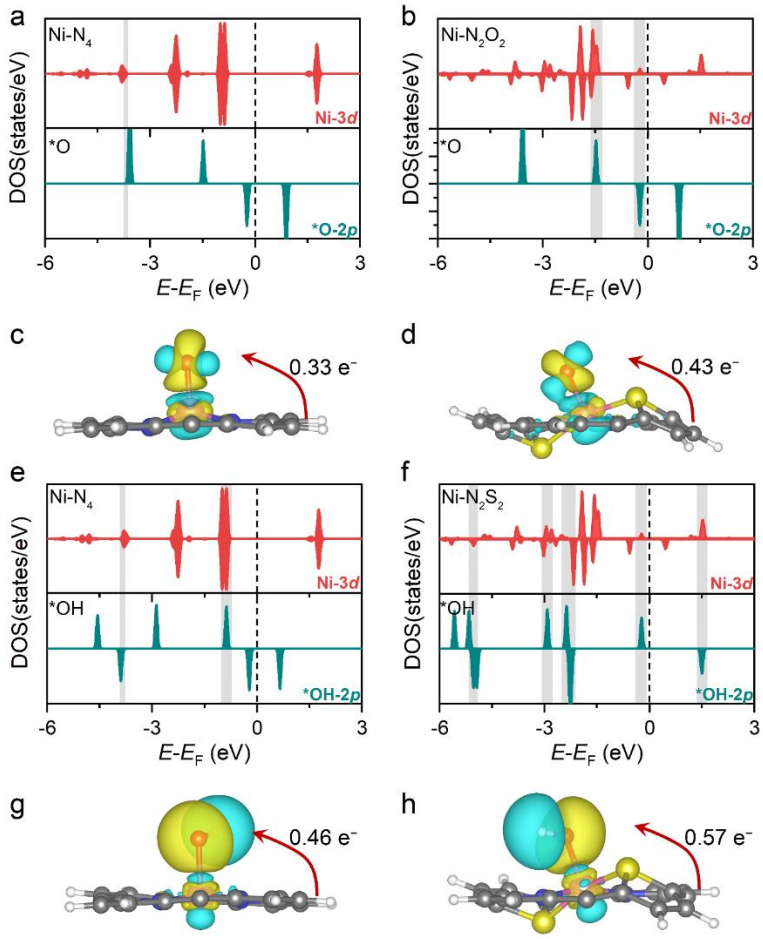

Figure S22. Projected electronic densities of states (PDOS) and charge density difference (CDD) of a-d) *O and e-h) *OH intermediates absorbed on Ni-N_4-, Ni-N_2S_2-Por-COFs. The cyan/yellow colors indicate the regions of electron loss/gain. Isosurfaces of charge density are set to 0.005 e Å $^{-3}$. For clarity, the tetraphenyl and the p-phenylenediamine (PPDA) moieties of M-$N_xO_yS_z$-Por-COFs are not shown.

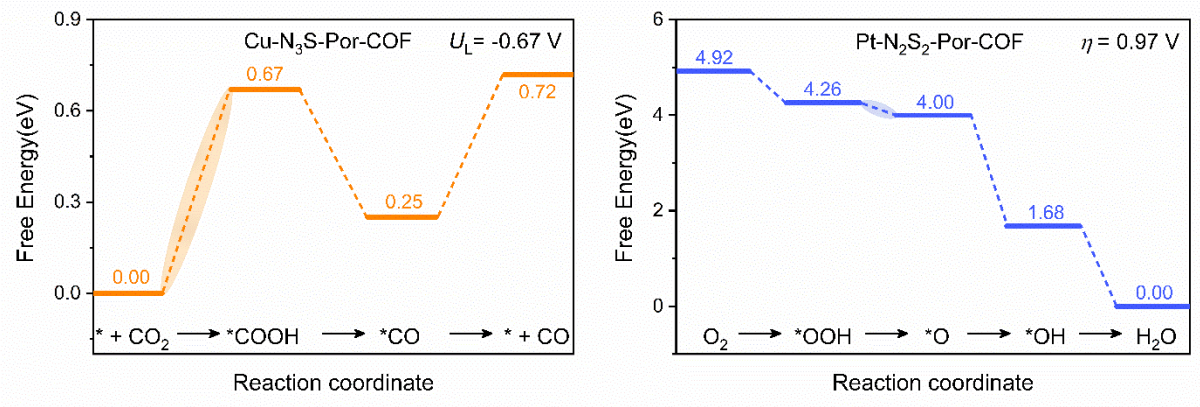

Figure S23. Free-energy diagram for a) CO_2RR-to-CO on Cu-N_3S-Por-COF and for b) ORR-to-H_2O on Pt-N_2S_2-Por-COF.

Supplementary Tables

Table S1. The values of U-J parameters for DFT/PBE+U calculations.

	Fe	Co	Ni	Cu	Pt
U-J	3.29	3.42	3.40	3.87	3.00

Table S2. Relative free energies (eV) with different magnetic moments M (μ_B) for the intermediates adsorbed on Fe-Por-COFs at 298.15 K. For each species, the most stable spin state is highlighted in bold. The optimized value of default-M is reported as M_{opt}.

	Fe-N_4-Por-COF				**Fe-N_3O-Por-COF**				**Fe-N_3S-Por-COF**			
	default	3	5	M_{opt}	default	3	5	M_{opt}	default	3	5	M_{opt}
G (*)	0.01	0.09	**0.00**	/	1.15	**0.00**	0.79	/	0.15	0.01	**0.00**	/
G (*COOH)	**0.00**	0.01	0.04	*-1.15*	0.06	**0.00**	0.06	/	**0.00**	0.13	0.01	*0.01*
G (*CO)	0.01	0.01	**0.00**	/	0.58	0.58	**0.00**	/	0.54	0.01	**0.00**	/
G (*H)	**0.00**	0.01	0.01	*1.19*	**0.00**	0.03	0.03	*-0.01*	**0.00**	0.02	0.04	*-0.01*
G(*OOH)	0.01	**0.00**	0.01	/	1.15	0.03	**0.00**	/	0.78	0.02	**0.00**	/
G(*O)	0.03	0.01	**0.00**	/	0.69	0.03	**0.00**	/	0.43	**0.00**	0.01	/
G(*OH)	0.01	0.01	**0.00**	/	1.40	0.01	**0.00**	/	0.96	**0.00**	0.01	/

	Fe-N_2O_2-Por-COF				**Fe-N_2S_2-Por-COF**				**Fe-N_2OS-Por-COF**			
	default	3	5	M_{opt}	default	3	5	M_{opt}	default	3	5	M_{opt}
G (*)	0.01	0.01	**0.00**	/	**0.00**	0.01	0.04	*1.62*	0.98	0.33	**0.00**	/
G (*COOH)	0.55	0.55	**0.00**	/	0.29	**0.00**	0.01	/	0.59	0.01	**0.00**	/
G (*CO)	0.80	0.80	**0.00**	/	0.47	0.01	**0.00**	/	0.66	0.66	**0.00**	/
G (*H)	**0.00**	0.48	0.09	*1.74*	**0.00**	0.08	0.04	*1.00*	0.13	0.13	**0.00**	/
G(*OOH)	**0.00**	0.02	0.06	*1.36*	0.82	0.69	**0.00**	/	0.75	0.01	**0.00**	/
G(*O)	0.35	**0.00**	0.36	/	0.38	0.01	**0.00**	/	0.34	**0.00**	0.02	/
G(*OH)	1.70	0.01	**0.00**	/	**0.00**	0.03	0.03	*3.00*	1.57	0.01	**0.00**	/

Table S3. Relative free energies (eV) with different magnetic moments M (μ_B) for the intermediates adsorbed on Co-Por-COFs at 298.15 K. For each species, the most stable spin state is highlighted in bold. The optimized value of default-M is reported as M_{opt}.

	Co-N$_4$-Por-COF				**Co-N$_3$O-Por-COF**				**Co-N$_3$S-Por-COF**			
	default	2	4	M_{opt}	default	2	4	M_{opt}	default	2	4	M_{opt}
G (*)	**0.00**	1.20	0.16	*-1.05*	0.12	0.12	**0.00**	/	0.01	0.19	**0.00**	/
G (*COOH)	**0.00**	0.02	0.01	*0.01*	0.01	**0.00**	0.01	/	0.01	**0.00**	0.01	/
G (*CO)	0.01	0.05	**0.00**	/	0.01	0.79	**0.00**	/	0.01	0.48	**0.00**	/
G (*H)	0.01	**0.00**	0.01	/	0.16	0.13	**0.00**	/	0.01	0.01	**0.00**	/
G(*OOH)	0.29	**0.00**	0.17	/	0.56	0.51	**0.00**	/	0.00	0.72	0.01	*4.77*
G(*O)	0.28	**0.00**	0.11	/	0.62	0.63	**0.00**	/	0.02	0.83	**0.00**	/
G(*OH)	0.25	0.01	**0.00**	/	0.74	0.81	**0.00**	/	0.02	0.74	**0.00**	/

	Co-N$_2$O$_2$-Por-COF				**Co-N$_2$S$_2$-Por-COF**				**Co-N$_2$OS-Por-COF**			
	default	2	4	M_{opt}	default	2	4	default	2	4	M_{opt}	4
G (*)	0.47	0.89	**0.00**	/	**0.00**	0.01	0.01	*1.00*	**0.00**	0.01	0.01	*1.08*
G (*COOH)	0.01	**0.00**	0.01	/	0.01	0.01	**0.00**	/	0.01	0.01	**0.00**	/
G (*CO)	0.01	**0.00**	0.01	/	0.01	**0.00**	0.01	/	0.40	0.00	0.01	/
G (*H)	**0.00**	0.01	0.01	*1.99*	**0.00**	0.01	0.01	*0.00*	**0.00**	0.01	0.01	*0.00*
G(*OOH)	0.02	0.76	**0.00**	/	0.01	0.01	**0.00**	/	**0.00**	0.68	0.64	*-0.01*
G(*O)	**0.00**	0.23	1.19	*-2.04*	0.03	0.06	**0.00**	/	0.01	0.01	**0.00**	/
G(*OH)	0.01	0.81	**0.00**	/	0.01	0.01	**0.00**	/	0.03	0.73	**0.00**	/

Table S4. Relative free energies (eV) with different magnetic moments M (μ_B) for the intermediates adsorbed on Ni-Por-COFs at 298.15 K. For each species, the most stable spin state is highlighted in bold. The optimized value of default-M is reported as M_{opt}.

	Ni-N_4-Por-COF			**Ni-N_3O-Por-COF**			**Ni-N_3S-Por-COF**		
	default	3	M_{opt}	default	3	M_{opt}	default	3	M_{opt}
G (*)	**0.00**	0.01	*0.01*	**0.00**	0.01	*3.49*	0.01	**0.00**	*/*
G (*COOH)	0.01	0.00	*/*	**0.00**	0.01	*-0.01*	**0.00**	0.46	*2.00*
G (*CO)	**0.00**	0.01	*0.01*	0.01	**0.00**	*/*	0.01	**0.00**	*/*
G (*H)	0.01	**0.00**	*/*	**0.00**	0.32	*-2.00*	**0.00**	0.45	*2.00*
G(*OOH)	0.01	**0.00**	*/*	**0.00**	0.40	*0.01*	**0.00**	0.34	*2.00*
G(*O)	**0.00**	0.33	*-4.05*	0.45	**0.00**	*/*	**0.00**	0.47	*3.00*
G(*OH)	**0.00**	0.01	*1.00*	0.01	**0.00**	*/*	**0.00**	0.41	*2.00*

	Ni-N_2O_2-Por-COF			**Ni-N_2S_2-Por-COF**			**Ni-N_2OS-Por-COF**		
	default	3	M_{opt}	default	3	M_{opt}	default	3	M_{opt}
G (*)	0.01	**0.00**	*/*	0.01	**0.00**	*/*	**0.00**	0.01	*0.27*
G (*COOH)	**0.00**	0.30	*3.00*	0.01	**0.00**	*/*	0.01	**0.00**	*/*
G (*CO)	**0.00**	0.01	*0.01*	**0.00**	0.01	*0.01*	0.01	**0.00**	*/*
G (*H)	**0.00**	0.14	*1.00*	**0.00**	0.01	*1.00*	0.01	**0.00**	*/*
G(*OOH)	**0.00**	0.01	*2.14*	**0.00**	0.01	*1.00*	0.04	**0.00**	*/*
G(*O)	0.01	**0.00**	*/*	0.29	0.00	*/*	0.33	**0.00**	*/*
G(*OH)	**0.00**	0.12	*3.00*	**0.00**	0.01	*1.00*	0.22	**0.00**	*/*

Table S5. Calculated zero-point energy (ZPE, eV) and entropic correction (TS, eV) of $*O_2$, *OOH, *O and *OH for Fe/Co/Ni-$N_xO_yS_z$-Por-COFs at T = 298.15K.

System	*OOH		*O		*OH	
	ZPE_{*OOH}	TS_{*OOH}	ZPE_{*O}	TS_{*O}	ZPE_{*OH}	TS_{*OH}
Fe-N_4	0.43	0.16	0.07	0.06	0.33	0.12
Fe-N_3O	0.42	0.21	0.06	0.08	0.33	0.13
Fe-N_3S	0.43	0.22	0.06	0.08	0.32	0.14
Fe-N_2O_2	0.43	0.22	0.06	0.08	0.33	0.14
Fe-N_2S_2	0.43	0.20	0.06	0.08	0.32	0.14
Fe-N_2OS	0.42	0.17	0.05	0.10	0.33	0.13
Co-N_4	0.45	0.13	0.06	0.08	0.35	0.09
Co-N_3O	0.40	0.13	0.06	0.07	0.32	0.15
Co-N_3S	0.41	0.24	0.06	0.08	0.33	0.13
Co-N_2O_2	0.42	0.21	0.06	0.07	0.34	0.11
Co-N_2S_2	0.42	0.23	0.04	0.11	0.33	0.13
Co-N_2OS	0.42	0.24	0.06	0.09	0.33	0.14
Ni-N_4	0.43	0.21	0.05	0.08	0.32	0.09
Ni-N_3O	0.42	0.21	0.05	0.08	0.33	0.11
Ni-N_3S	0.42	0.18	0.05	0.08	0.33	0.12
Ni-N_2O_2	0.43	0.20	0.05	0.09	0.33	0.12
Ni-N_2S_2	0.42	0.21	0.04	0.11	0.33	0.13
Ni-N_2OS	0.42	0.16	0.06	0.08	0.34	0.12

Table S6. Calculated zero-point energy (ZPE, eV) and entropic correction (TS, eV) of $*CO_2$, *COOH, *CO and *H for Fe/Co/Ni-$N_xO_yS_z$-Por-COFs at T = 298.15K.

System	*COOH		*CO		*H	
	ZPE_{*COOH}	TS_{*COOH}	ZPE_{*CO}	TS_{*CO}	ZPE_{*H}	TS_{*H}
Fe-N_4	0.61	0.23	0.19	0.10	0.18	0.02
Fe-N_3O	0.58	0.19	0.19	0.16	0.19	0.01
Fe-N_3S	0.62	0.19	0.18	0.11	0.18	0.01
Fe-N_2O_2	0.59	0.25	0.18	0.10	0.13	0.03
Fe-N_2S_2	0.59	0.18	0.19	0.15	0.14	0.04
Fe-N_2OS	0.58	0.27	0.18	0.18	0.18	0.01
Co-N_4	0.62	0.22	0.18	0.18	0.20	0.01
Co-N_3O	0.68	0.13	0.19	0.15	0.18	0.01
Co-N_3S	0.62	0.22	0.19	0.16	0.20	0.01
Co-N_2O_2	0.61	0.23	0.20	0.13	0.17	0.02
Co-N_2S_2	0.60	0.23	0.18	0.17	0.21	0.01
Co-N_2OS	0.62	0.15	0.19	0.10	0.18	0.01
Ni-N_4	0.62	0.22	0.22	0.16	0.17	0.03
Ni-N_3O	0.59	0.13	0.19	0.16	0.16	0.01
Ni-N_3S	0.59	0.23	0.18	0.12	0.16	0.02
Ni-N_2O_2	0.59	0.18	0.20	0.15	0.16	0.02
Ni-N_2S_2	0.60	0.23	0.19	0.15	0.16	0.01
Ni-N_2OS	0.60	0.23	0.19	0.10	0.17	0.02

Table S7. Hyperparameters of three machine learning algorithms.

Target Value	Algorithm	Hyperparameter
U_L^{CO2RR}	RFR	n_estimators=1000
	GBR	n_estimators=1000, learning_rate=0.002,
	XGBoost	n_estimators=1000, learning_rate=0.005, colsample_bytree=1, max_depth=10
η^{ORR}	RFR	n_estimitors=1000
	GBR	n_estimators=1000, learning_rate=0.004
	XGBoost	n_estimators=500, learning_rate=0.009, colsample_bytree=1, max_depth=5

Table S8. Calculated adsorption energy $\Delta E_{ads\_CO2}(CO_2)$, bond lengths and bond angle of $*CO_2$ absorbed on Fe/Co/Ni-$N_xO_yS_z$-Por-COFs.

Catalyst	ΔE_{ads_CO2} (eV)	Bond Length				Bond Angle	
		d_{C-O1} (Å)	Δ_1	d_{C-O2} (Å)	Δ_2	$\angle_{O-C-O}$ (°)	Δ_3
Fe-N_4	-0.22	1.18	*1.72%*	1.17	*0.86%*	179.32	*0.38%*
Fe-N_3O	-0.12	1.24	*6.90%*	1.22	*5.17%*	141.72	*21.27%*
Fe-N_3S	-0.11	1.18	*1.72%*	1.17	*0.86%*	179.82	*0.10%*
Fe-N_2O_2	-0.14	1.25	*7.76%*	1.25	*7.76%*	133.58	*25.79%*
Fe-N_2S_2	-0.19	1.17	*0.86%*	1.18	*1.72%*	179.40	*0.33%*
Fe-N_2OS	0.00	1.22	*5.17%*	1.26	*8.62%*	141.67	*21.29%*
Co-N_4	-0.25	1.18	*1.72%*	1.17	*0.86%*	179.63	*0.21%*
Co-N_3O	-0.34	1.24	*6.90%*	1.23	*6.03%*	138.94	*22.81%*
Co-N_3S	-0.12	1.18	*1.72%*	1.17	*0.86%*	179.64	*0.20 %*
Co-N_2O_2	-0.25	1.23	*6.03%*	1.21	*4.31%*	145.92	*18.93%*
Co-N_2S_2	0.02	1.18	*1.72%*	1.18	*1.72%*	179.85	*0.08%*
Co-N_2OS	-0.24	1.22	*5.17%*	1.21	*4.31%*	148.92	*17.27%*
Ni-N_4	-0.23	1.18	*1.72%*	1.18	*1.72%*	179.88	*0.07%*
Ni-N_3O	-0.12	1.21	*4.31%*	1.21	*4.31%*	148.64	*17.42%*
Ni-N_3S	-0.27	1.18	*1.72%*	1.18	*1.72%*	179.51	*0.27%*
Ni-N_2O_2	-0.18	1.21	*4.31%*	1.21	*4.31%*	148.45	*17.53%*
Ni-N_2S_2	-0.26	1.18	*1.72%*	1.18	*1.72%*	179.83	*0.09%*
Ni-N_2OS	-0.10	1.21	*4.31%*	1.21	*4.31%*	150.99	*16.12%*

Note:

$\Delta_{1\text{-}2}$ is the degree to which the C-O bond length of the adsorbed $*CO_2$-moiety changes with respect to the C-O bond length (1.16 Å) of the gas CO_2 molecule; Δ_3 is the degree to which the $\angle_{O-C-O}$ of the adsorbed $*CO_2$-moiety changes with respect to the $\angle_{O-C-O}$ (180°) of the gas CO_2 molecule.

$$\Delta_{1-2} = \left| \frac{d_{C-O}(*CO_2) - 1.16}{1.16} \right|$$

$$\Delta_3 = \left| \frac{\angle \mathrm{O-C-O}(*CO_2) - 180}{180} \right|$$

Table S9. Calculated adsorption energy, $\Delta E_{ads\text{-}O2}$, and bond lengths of $*O_2$ absorbed on Fe/Co/Ni-$N_xO_yS_z$-Por-COFs.

Catalyst	$\Delta E_{ads\text{-}O2}$	**Bond Length**	
		$d_{O\text{–}O}$ **(Å)**	Δ
Fe-N_4	-0.42	1.33	9.92%
Fe-N_3O	-1.41	1.43	18.18%
Fe-N_3S	-1.47	1.43	18.18%
Fe-N_2O_2	-1.58	1.42	17.36%
Fe-N_2S_2	-1.25	1.38	14.05%
Fe-N_2OS	-1.58	1.42	17.36%
Co-N_4	-0.22	1.24	2.48%
Co-N_3O	-1.57	1.34	10.74%
Co-N_3S	-1.14	1.34	10.74%
Co-N_2O_2	-1.28	1.34	10.74%
Co-N_2S_2	-0.77	1.33	9.92%
Co-N_2OS	-1.22	1.38	14.05%
Ni-N_4	-0.25	1.24	2.48%
Ni-N_3O	-0.82	1.32	9.09%
Ni-N_3S	-0.74	1.31	8.26%
Ni-N_2O_2	-0.74	1.32	9.09%
Ni-N_2S_2	-0.18	1.3	7.44%
Ni-N_2OS	-0.81	1.31	8.26%

Note:

Δ is the degree to which the O−O bond length of the adsorbed $*O_2$-moiety changes with respect to the O−O bond length (1.21 Å) of the gas O_2 molecule.

$$\Delta = \left| \frac{d_{C-O}(*O_2) - 1.21}{1.21} \right|$$

Table S10. The feature values of each Por-COF. The features include the atomic number (N^{atom}), the number of valence electron (n_e), the number of *d* electron (n_d), the covalent radius (r^{atom}, Å), the van der Waals radius (r^{vdw}, Å), the relative mass (*m*), the Pauling electronegativity (EN), the electron affinity (EA, eV), the first ionization energy (IE, eV) of the central metal atoms (n_N); the number of coordinated N atoms, the sum of valence electron count ($\sum n_e$), the sum of *p* electron ($\sum n_p$), the sum of covalent radius ($\sum r^{atom}$, Å), the sum of van der Waals radius ($\sum r^{vdw}$, Å), the sum of Pauling electronegativity ($\sum$ EN), the sum of electron affinity ($\sum$ EA, eV) of the coordination structures; the bond lengths of M−X_1 ($d_{M\text{-}X1}$, Å), M−X_2 ($d_{M\text{-}X2}$, Å), M−N_1 ($d_{M\text{-}N1}$, Å) and M−N_2 ($d_{M\text{-}N2}$, Å).

System	N^{atom}	n_e	n_d	r^{atom}	r^{vdw}	*m*	EN	EA	IE	n_N	$\sum n_e$	$\sum n_p$	$\sum r^{atom}$	$\sum r^{vdw}$	$\sum$ EN	$\sum$ EA	$d_{M\text{-}X1}$	$d_{M\text{-}X2}$	$d_{M\text{-}N2}$	$d_{M\text{-}N2}$
Fe-N_4	26.00	8.00	6.00	1.32	2.44	55.85	1.83	15.70	7.90	4.00	20.00	12.00	2.84	6.64	12.16	28.00	2.00	2.00	2.01	2.01
Fe-N_3O	26.00	8.00	6.00	1.32	2.44	55.85	1.83	15.70	7.90	3.00	21.00	13.00	2.79	6.48	12.56	162.00	2.23	2.00	2.03	2.03
Fe-N_3S	26.00	8.00	6.00	1.32	2.44	55.85	1.83	15.70	7.90	3.00	21.00	13.00	3.18	6.87	11.70	221.00	2.40	1.99	2.09	2.08
Fe-N_2O_2	26.00	8.00	6.00	1.32	2.44	55.85	1.83	15.70	7.90	2.00	22.00	14.00	2.74	6.32	12.96	296.00	2.18	2.18	2.01	2.01
Fe-N_2S_2	26.00	8.00	6.00	1.32	2.44	55.85	1.83	15.70	7.90	2.00	22.00	14.00	3.52	7.10	11.24	414.00	2.20	2.20	2.05	2.05
Fe-N_2OS	26.00	8.00	6.00	1.32	2.44	55.85	1.83	15.70	7.90	2.00	22.00	14.00	3.13	6.71	12.10	355.00	2.39	2.16	2.04	2.04
Co-N_4	27.00	9.00	7.00	1.26	2.40	58.93	1.88	63.70	7.88	4.00	20.00	12.00	2.84	6.64	12.16	28.00	1.98	1.98	1.99	1.99
Co-N_3O	27.00	9.00	7.00	1.26	2.40	58.93	1.88	63.70	7.88	3.00	21.00	13.00	2.79	6.48	12.56	162.00	2.17	1.95	1.96	1.96

Co-N_3S	27.00	9.00	7.00	1.26	2.40	58.93	1.88	63.70	7.88	3.00	21.00	13.00	3.18	6.87	11.70	221.00	2.15	1.94	2.02	2.02
Co-N_2O_2	27.00	9.00	7.00	1.26	2.40	58.93	1.88	63.70	7.88	2.00	22.00	14.00	2.74	6.32	12.96	296.00	2.16	2.16	1.95	1.95
Co-N_2S_2	27.00	9.00	7.00	1.26	2.40	58.93	1.88	63.70	7.88	2.00	22.00	14.00	3.52	7.10	11.24	414.00	2.17	2.17	2.04	2.04
Co-N_2OS	27.00	9.00	7.00	1.26	2.40	58.93	1.88	63.70	7.88	2.00	22.00	14.00	3.13	6.71	12.10	355.00	2.16	2.12	2.02	2.02
Ni-N_4	28.00	10.00	8.00	1.24	2.40	58.69	1.91	112.00	7.63	4.00	20.00	12.00	2.84	6.64	12.16	28.00	1.96	1.96	1.98	1.98
Ni-N_3O	28.00	10.00	8.00	1.24	2.40	58.69	1.91	112.00	7.63	3.00	21.00	13.00	2.79	6.48	12.56	162.00	2.25	1.97	1.98	1.97
Ni-N_3S	28.00	10.00	8.00	1.24	2.40	58.69	1.91	112.00	7.63	3.00	21.00	13.00	3.18	6.87	11.70	221.00	2.12	1.94	2.05	2.05
Ni-N_2O_2	28.00	10.00	8.00	1.24	2.40	58.69	1.91	112.00	7.63	2.00	22.00	14.00	2.74	6.32	12.96	296.00	2.17	2.16	1.95	1.95
Ni-N_2S_2	28.00	10.00	8.00	1.24	2.40	58.69	1.91	112.00	7.63	2.00	22.00	14.00	3.52	7.10	11.24	414.00	2.14	2.14	2.03	2.03
Ni-N_2OS	28.00	10.00	8.00	1.24	2.40	58.69	1.91	112.00	7.63	2.00	22.00	14.00	3.13	6.71	12.10	355.00	2.13	2.13	2.01	2.01

Table S11. The comparison of the training/test RMSE and R^2 scores of three algorithms in fourfold cross-validation for U_L^{CO2RR}. The ML model yielding a maximum accuracy is highlighted in bold.

Algorithm	Loop	Training RMSE(V)	Training R^2	Test RMSE(V)	Test R^2
RFR	1	0.09	0.88	0.19	0.35
	2	0.09	0.87	0.24	0.35
	3	0.08	0.92	0.22	0.18
	4	0.09	0.90	0.18	0.51
	Mean Value	*0.09*	*0.89*	*0.20*	*0.35*
GBR	1	0.06	0.95	0.22	0.34
	2	0.05	0.98	0.09	0.61
	3	0.03	0.98	0.27	0.49
	4	**0.05**	**0.96**	**0.12**	**0.81**
	Mean Value	*0.05*	*0.97*	*0.18*	*0.56*
XGBoost	1	0.03	0.98	0.23	0.43
	2	0.05	0.97	0.21	0.23
	3	0.04	0.97	0.17	0.38
	4	0.04	0.97	0.13	0.71
	Mean Value	*0.04*	*0.97*	*0.18*	*0.43*

Table S12. The comparison of the training/test RMSE and R^2 scores of three algorithms in fourfold cross-validation for η^{ORR}. The ML model yielding a maximum accuracy is highlighted in bold.

Algorithm	Loop	Training RMSE(V)	Training R^2	Test RMSE(V)	Test R^2
RFR	1	0.12	0.93	0.28	0.60
	2	0.16	0.88	0.29	0.41
	3	0.12	0.93	0.18	0.84
	4	0.14	0.90	0.29	0.57
	Mean Value	*0.14*	*0.91*	*0.26*	*0.61*
GBR	1	0.02	0.99	0.24	0.55
	2	0.02	0.99	0.23	0.70
	3	0.03	0.99	0.21	0.85
	4	0.01	0.99	0.33	0.50
	Mean Value	*0.02*	*0.99*	*0.25*	*0.65*
XGBoost	1	0.03	0.99	0.29	0.56
	2	0.04	0.99	0.26	0.53
	3	**0.04**	**0.99**	**0.07**	**0.98**
	4	0.04	0.99	0.15	0.92
	Mean Value	*0.04*	*0.99*	*0.19*	*0.74*

Table S13. Comparison of the ML-predicted and DFT-calculated U_L^{CO2RR} and η^{ORR} values.

System	U_L^{CO2RR}		η^{ORR}	
	ML-predicted	**DFT-calculated**	**ML-predicted**	**DFT-calculated**
Fe-N_4	-1.25	-1.26	0.66	0.65
Fe-N_3O	-1.24	-1.20	1.50	1.48
Fe-N_3S	-1.18	-1.13	1.60	1.58
Fe-N_2O_2	-0.66	-0.70	1.63	1.60
Fe-N_2S_2	-0.91	-0.86	1.46	1.39
Fe-N_2OS	-0.64	-0.70	1.62	1.58
Co-N_4	-0.89	-0.89	0.43	0.44
Co-N_3O	-0.67	-0.83	1.76	1.64
Co-N_3S	-0.74	-0.78	1.32	1.30
Co-N_2O_2	-0.58	-0.66	1.48	1.45
Co-N_2S_2	-0.88	-0.89	0.94	0.96
Co-N_2OS	-0.76	-0.78	1.32	1.36
Ni-N_4	-1.52	-1.43	0.78	0.75
Ni-N_3O	-1.35	-1.18	0.74	0.72
Ni-N_3S	-1.08	-1.10	0.51	0.63
Ni-N_2O_2	-0.98	-0.96	0.72	0.73
Ni-N_2S_2	-1.25	-1.16	0.46	0.46
Ni-N_2OS	-1.05	-1.09	0.63	0.63

Table S14. Feature importance analysis of optimal GBR model for U_L^{CO2RR} and XGBoost model for η^{ORR}.

U_L^{CO2RR}		η^{ORR}	
Feature	**Importance (%)**	**Feature**	**Importance (%)**
m	33.53	d_{M-X1}	56.01
d_{M-X2}	28.26	N^{atom}	27.47
$\sum$ EA	12.80	n_N	4.51
d_{M-X1}	3.54	m	4.41
d_{M-N2}	3.45	$\sum$ EA	3.70
d_{M-N1}	2.88	$\sum r^{atom}$	2.54
$\sum$ EN	1.96	d_{M-X2}	0.70
$\sum r^{vdw}$	1.73	d_{M-N2}	0.65
$\sum r^{atom}$	1.69	d_{M-N1}	< 0.01
r^{atom}	1.61	$\sum$ EN	< 0.01
IE	1.50	$\sum r^{vdw}$	< 0.01
EN	1.47	r^{atom}	< 0.01
n_e	1.41	IE	< 0.01
n_d	1.29	EN	< 0.01
EA	1.25	n_e	< 0.01
N^{atom}	1.22	n_d	< 0.01
r^{vdw}	0.17	EA	< 0.01
$\sum n_e$	0.10	r^{vdw}	< 0.01
n_N	0.08	$\sum n_e$	< 0.01
$\sum n_p$	0.06	$\sum n_p$	< 0.01
Total	100	Total	100

Table S15. The ML-predicted or DFT-calculated U_L^{CO2RR} and η^{ORR} values for Cu-/Pt/Co-embedded Por-COFs.

System	ML-predicted		System	DFT-calculated	
	U_L^{CO2RR}	η^{ORR}		U_L^{CO2RR}	η^{ORR}
Cu-N_4	-0.88	0.75			
Cu-N_3O	-0.85	0.74			
Cu-N_3S	-0.81	0.64	Cu-N_3S	-0.67	/
Cu-N_2O_2	-0.91	0.74			
Cu-N_2S_2	-0.96	0.64			
Cu-N_2OS	-0.91	0.65			
Pt-N_4	-0.88	0.75			
Pt-N_3O	-0.83	0.74			
Pt-N_3S	-0.82	0.64			
Pt-N_2O_2	-0.82	0.73			
Pt-N_2S_2	-0.95	0.64	Pt-N_2S_2	/	0.97
Pt-N_2OS	-0.88	0.64			
Co-N_3C_1	-1.00	/	Co-N_3C_1	-0.76	/
Co-N_2C_2	-0.98	/	Co-N_2C_2	-0.60	/

Reference

1 A. Peterson and J. K. Nørskov, Activity Descriptors for CO_2 Electroreduction to Methane on Transition-Metal Catalysts, *J. Phys. Chem. Lett.*, 2012, **3**, 251–258.

2 Z. Ni, H. Liang, Z. Yi, R. Guo, C. Liu, Y. Liu, H. Sun and X. Liu, Research progress of electrochemical CO_2 reduction for copper-based catalysts to multicarbon products, *Coord. Chem. Rev.*, 2021, **441**, 213983.

3 M. Liu, Z. Zhao, X. Duan and Y. Huang, Nanoscale Structure Design for High-Performance Pt-Based ORR Catalysts, *Adv. Mater.*, 2019, **31**, 1802234.

4 K. Kodama, T. Nagai, A. Kuwaki, R. Jinnouchi and Y. Morimoto, Challenges in applying highly active Pt-based nanostructured catalysts for oxygen reduction reactions to fuel cell vehicles, *Nat. Nanotechnol.*, 2021, **16**, 140–147.

5 Z. Ren, B. Zhao and J. Xie, Designing N-Confused Metalloporphyrin-Based Covalent Organic Frameworks for Enhanced Electrocatalytic Carbon Dioxide Reduction, *Small*, 2023, **19**,2301818.

6 S. Lin, C. S. Diercks, Y.-B. Zhang, N. Kornienko, E. M. Nichols, Y. Zhao, A. R. Paris, D. Kim, P. Yang, O. M. Yaghi and C. J. Chang, Covalent organic frameworks comprising cobalt porphyrins for catalytic CO2 reduction in water, *Science*, 2015, **349**, 1208–1213.

7 S. An, C. Lu, Q. Xu, C. Lian, C. Peng, J. Hu, X. Zhuang and H. Liu, Constructing Catalytic Crown Ether-Based Covalent Organic Frameworks for Electroreduction of CO_2, *ACS Energy Lett.*, 2021, **6**, 3496–3502.

8 S. Diercks, S. Lin, N. Kornienko, E. A. Kapustin, E. M. Nichols, C. Zhu, Y. Zhao, C. J. Chang and O. M. Yaghi, Reticular Electronic Tuning of Porphyrin Active Sites in Covalent Organic Frameworks for Electrocatalytic Carbon Dioxide Reduction, *J. Am. Chem. Soc.*, 2018, **140**, 1116–1122.

9 H.-J. Zhu, M. Lu, Y.-R. Wang, S.-J. Yao, M. Zhang, Y.-H. Kan, J. Liu, Y. Chen, S.-L. Li and Y.-Q. Lan, Efficient electron transmission in covalent organic framework nanosheets for highly active electrocatalytic carbon dioxide reduction, *Nat. Commun.*, 2020, **11**, 497.

10 Q. Wu, M.-J. Mao, Q.-J. Wu, J. Liang, Y.-B. Huang and R. Cao, Construction of Donor–Acceptor Heterojunctions in Covalent Organic Framework for Enhanced CO2 Electroreduction, *Small*, 2021, **17**, 2004933.

11 Q. Wu, R.-K. Xie, M.-J. Mao, G.-L. Chai, J.-D. Yi, S.-S. Zhao, Y.-B. Huang and R. Cao, Integration of Strong Electron Transporter Tetrathiafulvalene into Metalloporphyrin-Based Covalent Organic Framework for Highly Efficient Electroreduction of CO_2, *ACS Energy Lett.*, 2020, **5**, 1005–1012.

12 Y. Lu, J. Zhang, W. Wei, D. Ma, X. Wu and Q. Zhu, Efficient Carbon Dioxide Electroreduction over Ultrathin Covalent Organic Framework Nanolayers with Isolated Cobalt Porphyrin Units, *ACS Appl. Mater. Interfaces*, 2020, **12**, 37986–37992.

13 M. Fang, L. Xu, H. Zhang, Y. Zhu and W.-Y. Wong, Metalloporphyrin-Linked Mercurated Graphynes for Ultrastable CO_2 Electroreduction to CO with Nearly 100% Selectivity at a Current Density of 1.2 A cm^{-2}, *J. Am. Chem. Soc.*, 2022, **144**, 15143–15154.
14 T. He, C. Yang, Y. Chen, N. Huang, S. Duan, Z. Zhang, W. Hu and D. Jiang, Bottom-Up Interfacial Design of Covalent Organic Frameworks for Highly Efficient and Selective Electrocatalysis of CO_2, *Adv. Mater.*, 2022, **34**, 2205186.
15 H. Dong, M. Lu, Y. Wang, H.-L. Tang, D. Wu, X. Sun and F.-M. Zhang, Covalently anchoring covalent organic framework on carbon nanotubes for highly efficient electrocatalytic CO_2 reduction, *Appl. Catal. B Environ.*, 2022, **303**, 120897.